REPUBLIQUE ALGERIENNE DEMOCRATIQUE ET POPULAIRE

MINISTERE DE L'ENSEIGNEMENT SUPERIEUR ET DE LA RECHERCHE SCIENTIFIQUE

UNIVERSITE MOHAMED BOUDIAF - M'SILA

FACULTE DES SCIENCES

DEPARTEMENT PHYSIQUE

N° : Ph/ENR/07/2023

DOMAINE : Sciences de la matière

FILIERE : Physique

OPTION : Physique Énergétique et Energie renouvelable

Mémoire présenté pour l'obtention
Du diplôme de Master Académique

Par: Brahimi Nouha

Intitulé

Numerical computation of geometric parameters effects on the solar chimney performance

Soutenu le 08 / 06 /2023 devant le jury composé de:

Dr Kalli Sihem	Université Mohamed Boudiaf- M'sila	Présidente
Dr Boulechfar Hichem	Université Mohamed Boudiaf- M'sila	Rapporteur
Pr Mayouf Si Abdellah	Université Mohamed Boudiaf- M'sila	Examinateur

Année universitaire : 2022/2023

Dedications

This work is wholeheartedly dedicated to my beloved parents who taught me to be unique and determined.

To my brothers and sisters who shared their words of advice and encouragement to help accomplish this study.

Acknowledgments

I would like to express my deepest appreciation to my supervisor **Dr. Boulechfar Hichem** for his invaluable patience and feedback.

My sincere thanks to **Pr. Mayouf Si Abdallah** and **Dr. Kalli Sihem** for accepting to be part of my master's defense jury.

This endeavour would not have been possible without the generous support of my precious family. Their faith in me has kept my spirit and motivation resilient throughout this journey.

Table of Contents

Nomenclature

Roman letters:

T_h	Hot temperature	[K]
T_c	Cold temperature	[K]
h	Chimney's height	[m]
P	Pressure	[Pa]
r, θ, z	Cylindrical coordinate	[m]
H	Collector height	[m]
D	Collector diameter	[m]
t	Time	[s]
g	Gravitational acceleration	[m/s^2]
Cp	Specific heat capacity	[$J.kg^{-1}.\ k^{-1}$]
v	Velocity	[m/s]
Pr	Prandtl number, $= \frac{v}{\alpha}$	
Ra	Rayleigh number, $= \frac{g\,\beta\,\Delta T\,D^3}{\upsilon\,\alpha}$	
v_r	Velocity component in (r) direction	[m/s]
v_z	Velocity component in (z) direction	[m/s]
v_θ	Velocity component in (θ) direction	[m/s]
r^+	Dimensionless radial coordinates	
z^+	Dimensionless z coordinates	
T^+	Dimensionless temperature	
P^+	Dimensionless pressure	
$v_r{}^+$	Dimensionless velocity component	
$v_z{}^+$	Dimensionless velocity component	
$v_\theta{}^+$	Dimensionless velocity component	

Greek letters:

β_T	Coefficient of thermal expansion	[1/K]
ρ	Density of the fluid	[kg/m]
λ	Thermal conductivity	[w/m. k]
α	Thermal diffusivity	[m^2 /s]
μ	Dynamic viscosity	[kg. m^{-1} .s^{-1}]
υ	Kinematic viscosity	

Subscripts:

r, θ, z	Cylindrical coordinate

Superscripts:

+	Dimensionless

List of figures

Chapter I

Chapter II

Chapter III

Chapter IV

INTRODUCTION

Due to the widespread use of conventional energies like coal, petroleum, and gas, which are believed to be the primary drivers behind the rapid growth of the twenty-first century economy, the world's energy consumption rates are rising along with health and environmental risks and increased greenhouse gas emissions.

The greatest companies in the world have explored innovative approaches to diversify their energy sources and discover suitable alternatives to improve energy security, minimize the risks associated with conventional energies, and lower production costs as a result of the complexity and dangers associated with resource acquisition, therefore scientists have shed light on green and renewable energies due to the wide variety of its resources (solar, biomass, tidal, hydrogen, wind, and geothermal) as a competitive alternative to conventional energies, including solar energy as a reliable and cost-free source.

One of the technologies for exploiting solar power is the solar chimney technology with working principle based on the free convection phenomenon resulting from the fluid density gradient, this impact brought on by the system's temperature difference between the ground and the collector, the airflow is consequently produced in the enclosure and moves up to drive the turbines which is responsible for generating electricity.

Our numerical study is focused on the effect of different geometrical proprieties of the solar chimney like collector’s height and junction curvature radius and how they impact the performance of the solar chimney through their impact on the airflow development.

The manuscript is presented as follows:

In the first chapter, which is titled as “Solar chimney overview and literature review” containing a global overview of some renewable energies and focused on the solar energy technology to delve gradually into the solar chimney technology than we conclude the chapter with a literature review and some previous studies concerning the subject.

The second chapter entitled “Modeling and problem formulation”, starts with introducing the problem as bi-dimensional axisymmetric solar chimney represented as a schematic figure to clarify the geometry with better details.

Then we delve into the problem description with governing equations in cylindrical coordinate using the boussinesq approximation while taking into account suitable assumptions and mathematical formalisms to simplify the studied case.

The third chapter concerns the numerical simulation software; we included a quick overview of the Comsol Multiphysics software and the numerical simulation procedures for resolving the problem's fundamental equations, citing a simple definition of the finite element method which is regarded as the base meshing method of the software.

In the last chapter, we illustrate different results with interpretation and discussion.

At the end we presented a conclusion that highlights the main results.

CHAPTER I

SOLAR CHIMNEY OVERVIEW AND LITERATURE REVIEW

I. Solar chimney overview

I.1 Introduction

In order to achieve environmental and social comfort, electrical effectiveness and economic development, scientists have long recognized renewable energies as a green, clean and sustainable alternative to fossil and nuclear energies because of their harmful emissions impact to the environment and safety issues to the society.

Renewable energies such as hydro-power, fuel cell energy, wind power and solar power technology has played a crucial part in achieving electrical efficiency by converting solar radiations either directly using photovoltaic technology or indirectly using thermal technology.

Among the most crucial systems for converting solar thermal energy into usable forms is the solar chimney, which primarily consists of three fundamental parts, The collector, the chimney also named tour, and turbines. The greenhouse effect heats the air inside the collector by absorbing sun radiations and the buoyancy effect creates a pressure difference between the warm air underneath and surrounding the collector. The airflow is consequently produced and enters the chimney; this provides a power generation by driving the turbines that are situated in the centre of the chimney.

I.2 Renewable energy conversion system

Sustainable energy efficiency has always been the focus of a lot of energy engineers through the centuries. Renewable energy systems are defined as being derived from natural and permanent sources that do not diminish and terminate over time.

I.2.1 Wind energy

Wind energy is one of the greatest potential energy alternatives and could also be regarded as eco-friendly for all alternatives. Wind power is produced from an unlimited and uneven source that is wind, which is originally caused by differences in pressure through the surfaces of the earth due to uneven heating by sunlight radiation.

Wind turbines generate power by turning the kinetic energy of air motion into electricity. The rotor blades are rotated by the wind, converting kinetic energy into rotational energy, this rotational energy is transmitted to the generator through a shaft resulting in the generation of

an electrical energy. The potential amount of energy of the wind is determined by the control of the size of the turbine and the length of its blades. **[1]**

Figure 1 : Wind turbines **[2]**

I.2.2 Bio energy

Earlier from now, biomass has always used as a survival source of energy in cooking and warming using firewood and coal. Scientists have classified this type of energy as a renewable power that means any source of thermal energy mainly generated from non-fossil biological and living organisms like plants and animals originally extracted from marine, freshwater and land-based habitats to produce heat, electricity and biofuels.

Biomass based transport fuels are highly dominants such as ethanol mainly extracted from corn and sugarcanes, in the other hand biodiesel fuel extracted from rapeseeds, palm oil and soy seeds in order to supply the worldwide demand of gasoline and diesel fuels. The prospects for ethanol energy from plants and several tree species depend on the cellulosic processing which remains to be demonstrated **[3]**.

Table 1 : Products depending on feedstock **[4]**

	Solid	**Liquid**	**Gaseous**
Wet feedstock	Briquette	Ethanol	Biogas
Dry feedstock	Fuel wood	Methanol	Producer gas

Wood, charcoal, crop and forestry residues are considered as solid fuels, agro-industrial and municipal wastes and briquettes. Gases are primarily biogas generated by anaerodigesters **[4]**.

Figure 2: Feedstock **[5]**

Figure 3: Briquettes **[5]**

Biomass can be directly converted into energy using a process known as gasification. During gasification, a biomass raw material is heated using a controlled quantity of oxygen, this gasifying factory in Maui, Hawaii, converts sugar cane into electricity **[5]**.

I.2.3 Hydro energy

The energy of flowing water is converted into electricity by hydroelectric power plants. The majority of public hydropower systems use a dam on a river to store a huge volume of water goes through turbines to generate power.

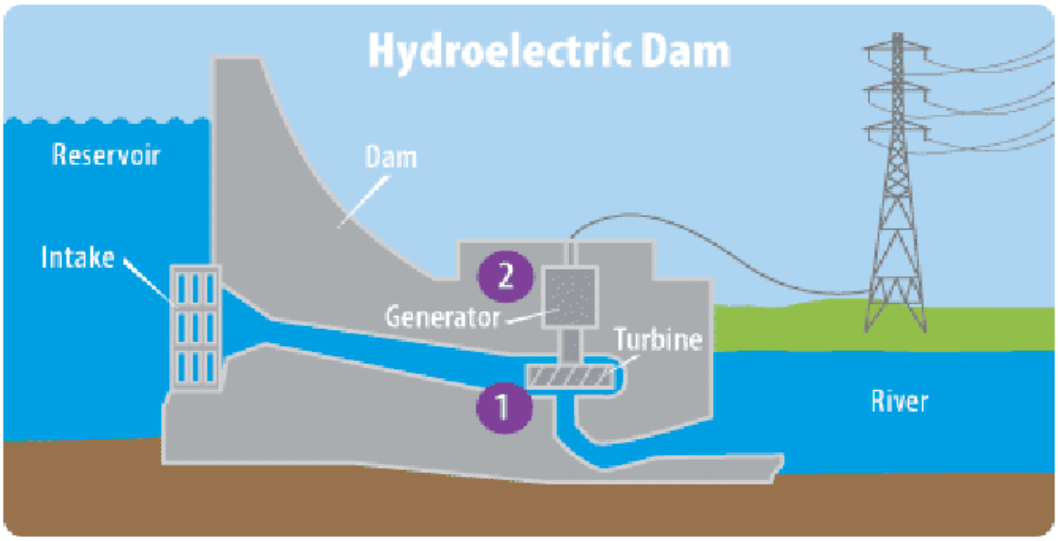

Figure 4: A diagram of a hydroelectric dam **[6]**

I.2.4 Fuel cell energy

In general, fuel cell technology is an electro-chemical technique for producing electricity that consists of an anode, a cathode, and an electrolyte membrane. The hydrogen molecules are divided into electrons and protons by sending hydrogen through the anode of a fuel cell and oxygen via the cathode. These final ones flow through the electrolyte membrane as the electrons are driven through a circuit, producing an electric current and surplus heat. Protons, electrons, and oxygen mix at the cathode to form water molecules **[7]**.

I.2.5 Solar energy

- **Origins**

The sun is a giant flaming ball and the star of the solar system, the closest to our planet with approximately diameter of 1.39 x 10^9 meters and 150 million (km) distance from earth.

The nuclear fusion reaction that occurs into the sun's core is mainly responsible for the energy supply whereby four atoms of hydrogen fuse together forming one helium atom. Astrophysicists found that the temperature in the inner core reach around 15 million degrees Celsius and pressure equal to 300,000 million times our atmosphere It then gradually drops to 2 million degrees Celsius in the interface layer of the radiative zone (tachocline) until it reaches about 5,800 K at the surface **[8]**.

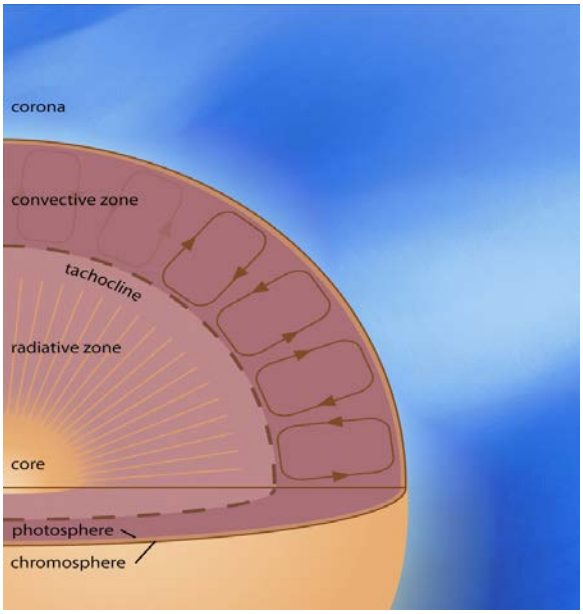

Figure 5: The sun's composition **[8]**

Solar energy manifests at the sun's surface as electromagnetic radiation with a total power output of 3.8 x 10^{20} MW and only a percentage of the solar radial beam penetrates the surface of the globe, which is the sum of three main radiations (diffused and reflected and direct radiations).

I.3 Solar energy technology

A variety of technologies over time has been in use to produce electricity and solar energy was considered the most crucial among them, it is a technology that essentially generates

electricity by converting solar radiation, or to provide thermal comfort and warmth within buildings whether directly or indirectly exploited.

I.3.1 Photovoltaic system

The term photovoltaic refers to the direct conversion of the photons emitted by the sunlight (solar radiations) into electric power under the photoelectric effect observed back in 1839 by the scientist Edmund Becquerel.

The concept of the process is using semi-conductor panels to generate electricity, when the semi-conductor material atoms start moving towards the panel after receiving a kinetic energy once the photons strike its surface.

Figure 6: Solar panel **[9]**

I.3.2 Thermal system

The indirect conversion process of solar sunlight to heat energy is the thermal technology system among the simplest alternatives with high potential to be exploited; it allows for the heating and production of hot water with metal sensors absorbing sunlight and transferring it to the coolant. It may also be used in dehydrating and evaporating by heat or generating electrical energy using a hybrid system of solar energy and turbines in which we may call solar chimneys.

I.3.2.1 Thermal energy for heating and drying

This system may be classified under two types of collectors, the flat plate low temperature collectors of around 60 degree Celsius to 100 degrees and Medium-temperature collectors generally used to heat swimming pools and buildings for air conditioning or ventilation.

I.3.2.2 Thermal energy for large scale conversion

This system is used for high- temperature collectors that take large areas and surfaces to harvest a significant amount of heat by capturing the sun's energy with aide of mirrors to reflect and focus the sunlight onto a receiver or absorber, generating heat that is then utilized to generate electricity using 5 different technologies, parabolic trough systems, power tower systems, linear Fresnel reflector systems and dish/engine systems as shown in figure; and the solar chimney power system.

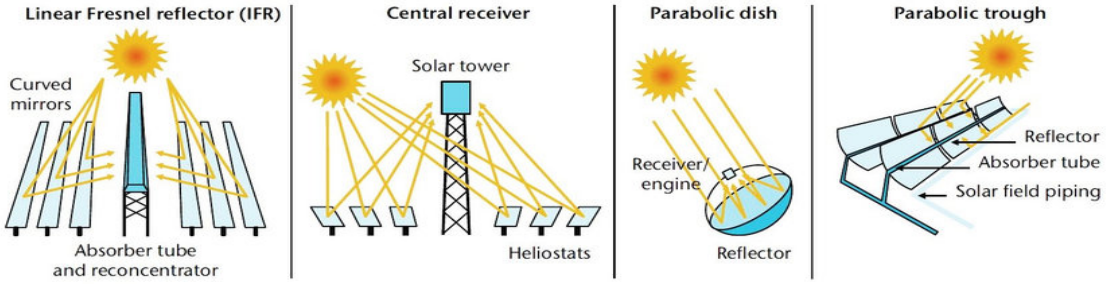

Figure 7: Solar thermal technologies **[10]**

- **Solar chimney power plants**

This is another form of solar thermal plant that has lately received attention from researchers as a clean alternative to solar energy generation that depends on the conversion of solar energy to electric energy based on the phenomenon of natural convection caused by heat transfer, which we will focus on in our research.

I.4 Solar chimney history and definition

I.4.1 A brief history

Owing to a research done by **Al-Kayiem et al, Leonardo Da Vinci** was the first to devise a rotating mechanism that incorporated a chimney and a windmill in ancient times in Figure 8. The windmill is linked to a roasting spit, which rotates as the windmill is turned by rising hot air, and is used to cook the chicken.

Earlier, precisely in the 20th century in 1903.The Spanish colonel **Isidoro Cabanyes** was first to describe the concept of the solar chimney presenting his (solar engine project) in order to generate electrical energy.

Back in 1968, the German engineer **Jörg Schlaich** proposed the Solar chimney power plant (SCPP) technology then presented it in the 1970s, and from 1980s to 1989 the project

prototype of a solar chimney in Mansanares Spain was successfully installed and operated until it was officially out of service **[11]**.

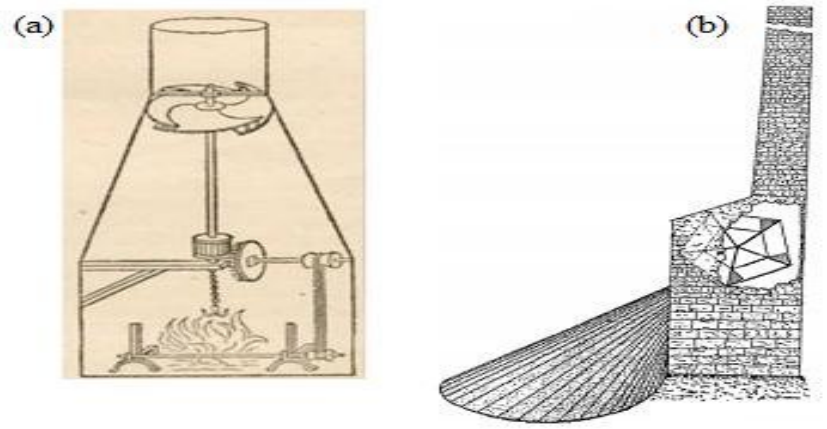

Figure 8: (a) represents the **Da Vinci**'s barbeque, (b) represents **Isodoro**'s project diagram **[11]**

I.4.2 Description

Among the applicable solar thermal technologies that converse solar radiations to electrical energy by the heat transfer process. Solar chimneys or called solar towers, a large scale system of heating cooling utility used to provide a ventilation and thermal comfort in buildings as shown in figure 9 and also a power generator by combining a hybrid system consist mainly of solar energy and turbines in a vertical tower called chimney.

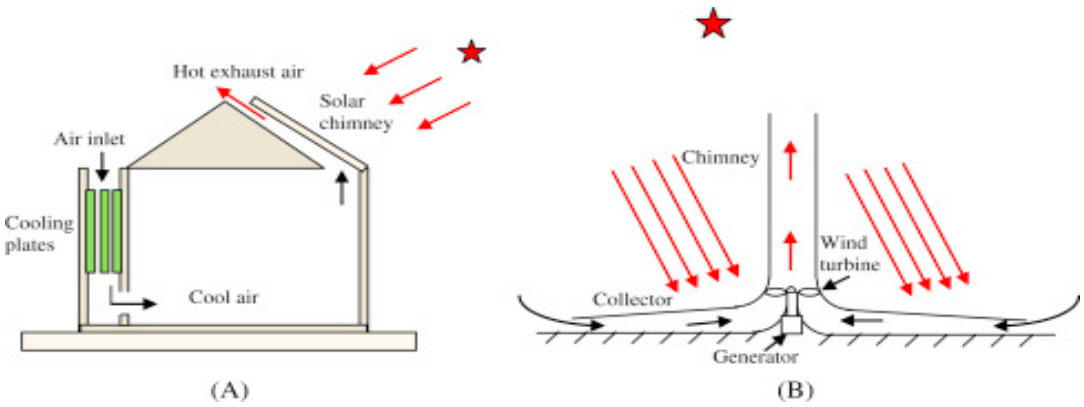

Figure 9: Solar chimney Applications **[12]**

I.5 Basic components of solar chimneys

The system is made up of three main parts: the chimney, the collector and the turbine.

I.5.1 The collector

The Solar collector consists of support matrix, column structure, and transparent roof either glazed or made of plastic **[13]**, when sunlight penetrates the transparent cover it directly converted to a thermal energy inciting the production of hot air by the greenhouse effect. It is classified as a large-scale thermal technology because it requires a huge area for the collector; the larger the area, the more energy is generated.

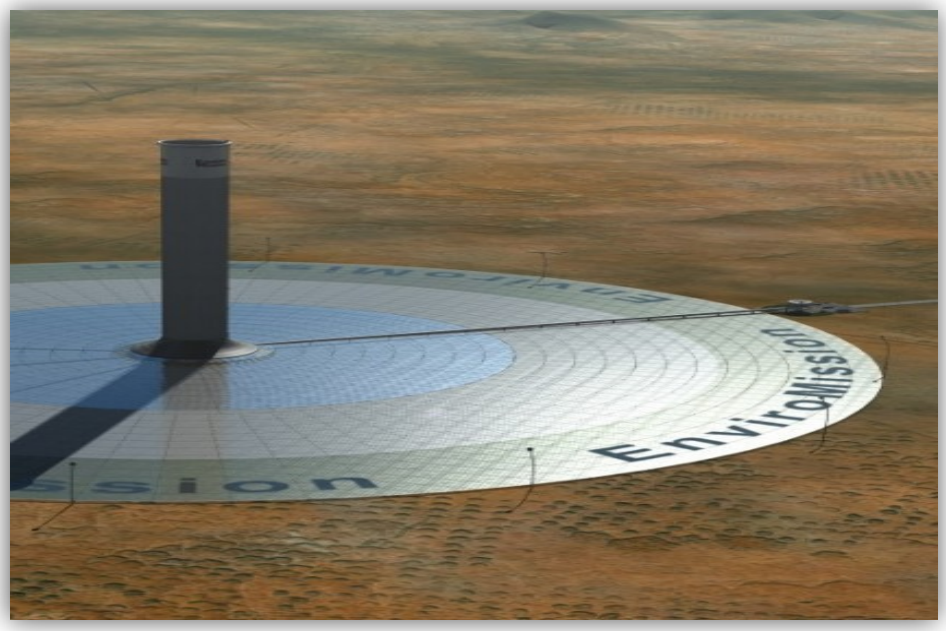

Figure 10: SCPP model collector **[14]**

I.5.2 The chimney

The tower of the solar chimney considered as the thermal engine of the system, placed mainly in the center of the collector, might be described as a large vertical tube channel that drives the warmed air by the collector outside the system through the outlet while the efficiency increases with the height of the chimney.

Figure 11: Tower model in Arizona project **[14]**

I.5.3 The turbine

The turbines are the main core of the system whereby electricity is generated, the warmed air in the collector goes directly upwards the chimney by the buoyancy effect to drive these turbines that convert the rotational energy to an electrical energy.

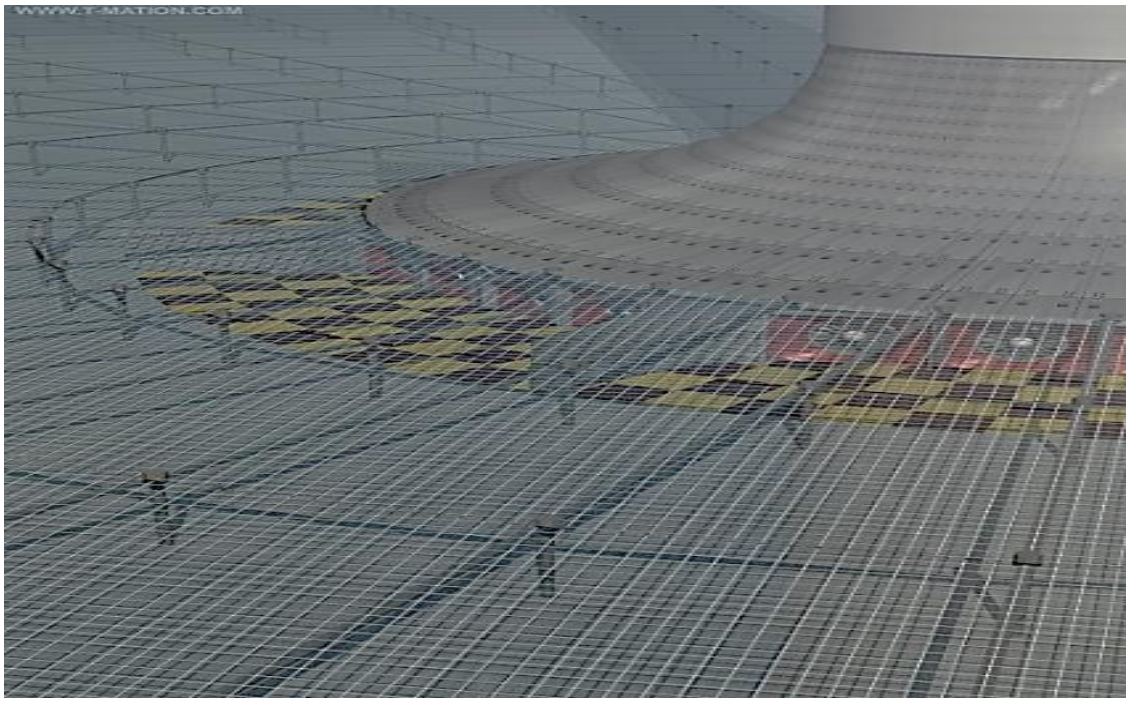

Figure 12: Turbines in a solar chimney **[14]**

I.6 Working principles

Solar thermal chimneys all use the same operating mechanism, which is based on the phenomena of naturel convection heat transfer caused by the solar heated collector to the atmospheric air **[15]**. Therefore buoyancy forces are resulted.

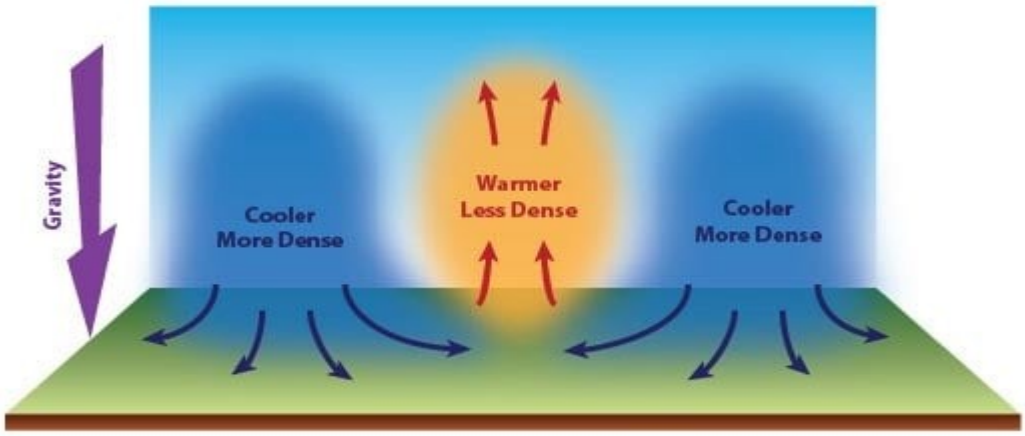

Figure 13: Buoyancy effect in natural convection **[16]**

When utilised in structures, these chimneys are frequently located on the roof top or the wall in the shape of tower. Their basic function is to refresh the air within buildings and rooms by drawing the less dense air outside the buildings through the tower, the tower's position performances determined by environmental factors, the most important of which are the wind directions and its efficiency is restrained by the towers height and the upcoming wind velocity.

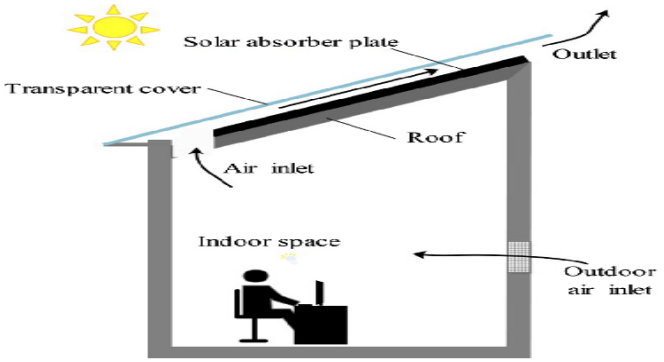

Figure 14: Schematic diagram of roof chimney **[18]**

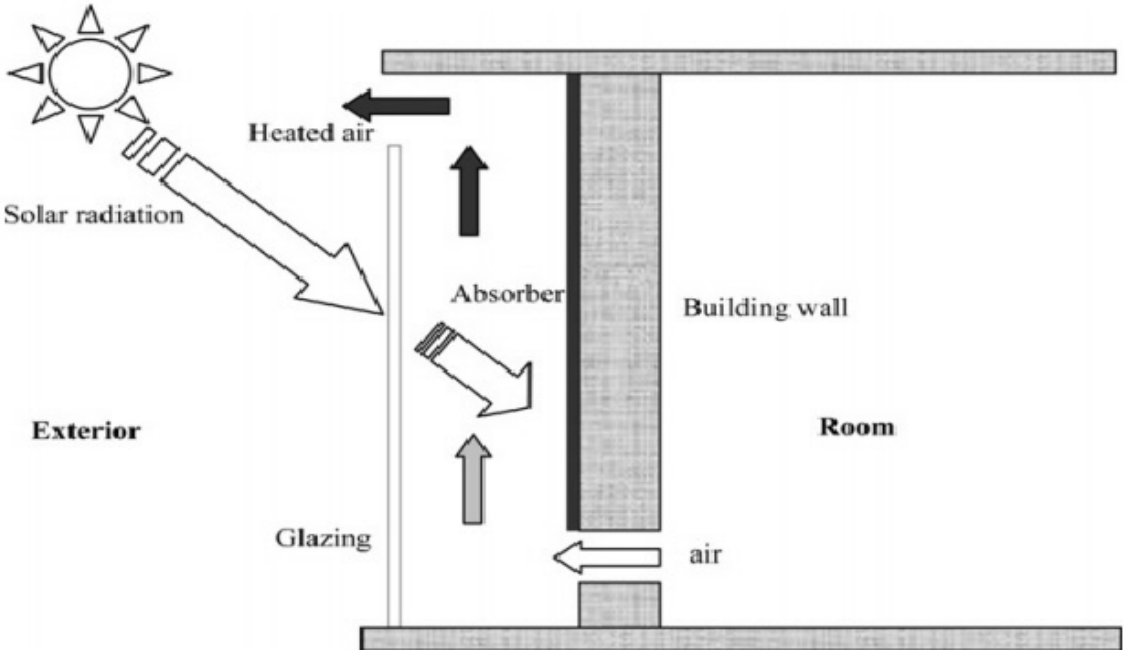

Figure 15: Schematic diagram of wall solar chimney **[17]**

To generate energy the chimney is paired with a turbines, the rising air currents cause these turbines to spin. Generators generate electricity by converting the rotational energy of turbines; the efficiency of their performance depends on the intensity of solar radiation and the air gap between the absorber wall and the glass roof of the collector **[19]**, as shown in figure (16).

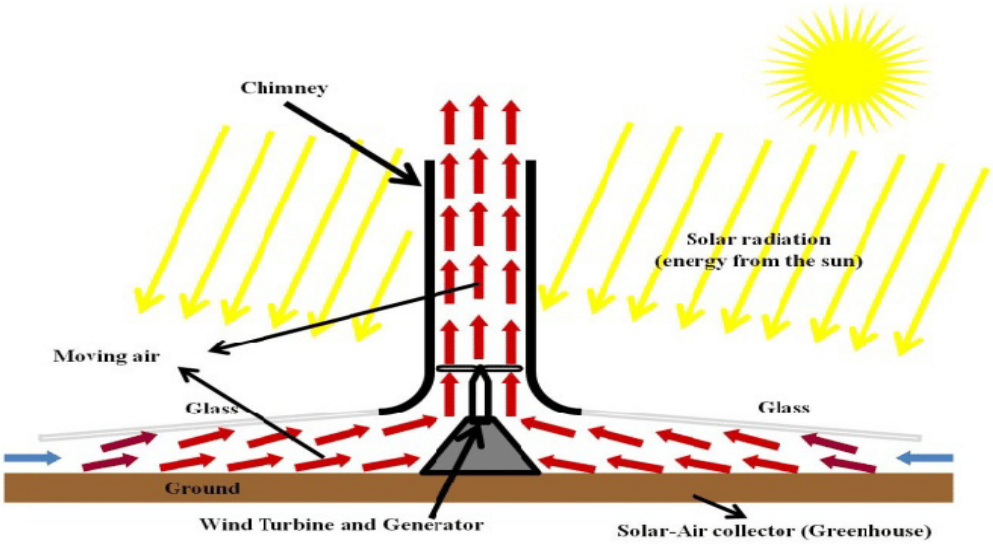

Figure 16: Schematic diagram of SCPP **[20]**

I.7 Solar chimney merits and demerits

I.7.1 Merits:

- Alternative solution to provide electricity in isolated and desert areas.
- Continuous daily power generation without interruption due to the availability of the natural storage system on the collector floor at night.
- No consumption of resources while operating.
- Inexhaustible and gratuitous source of energy. With no emissions of pollutants.
- The Solar Tower has high reliability and low maintenance compared to other power plants.
- It does not require any cooling system and it can be used in extreme drying areas.

I.7.2 Demerits:

- Requires appropriate technical expertise and the availability of construction resources backed by solid.
- Requires a very large land spaces.
- According to some statistics, using a solar chimney to generate power is more expensive than using a gas turbine.
- Solar chimneys require a high initial investment.

I.8 Solar chimney types

Solar chimneys are classified as conventional and non-conventional, depending on their purpose of use and their concept:

I.8.1 Conventional types

I.8.1.1 Power producing solar chimney

The majority of solar chimney technologies now in use are traditional solar chimney power plants, where the goal is to use one or more turbines installed inside the chimney to convert the kinetic energy of the rising air flow into electricity. To maximize the conversion of the ambient cold air into hot air in these conditions, solar collectors are often used as greenhouses around the tower.

I.8.1.2 Wall solar chimney

The wall solar chimney, also called trombe wall, generally it is used for winter heating and summer cooling, and it is built with an interior storage wall and external glass. The exterior glazing permits solar radiation to heat the chimney interior by accessing the interior. Then, air in the chamber rises due to thermal buoyancy. Under buoyancy drive, air enters the space through the top hole. The bottom-left hole allows for air exchange with the outside environment, while the bottom-right hole allows for air exchange with the inside space figure (17) **[21]**.

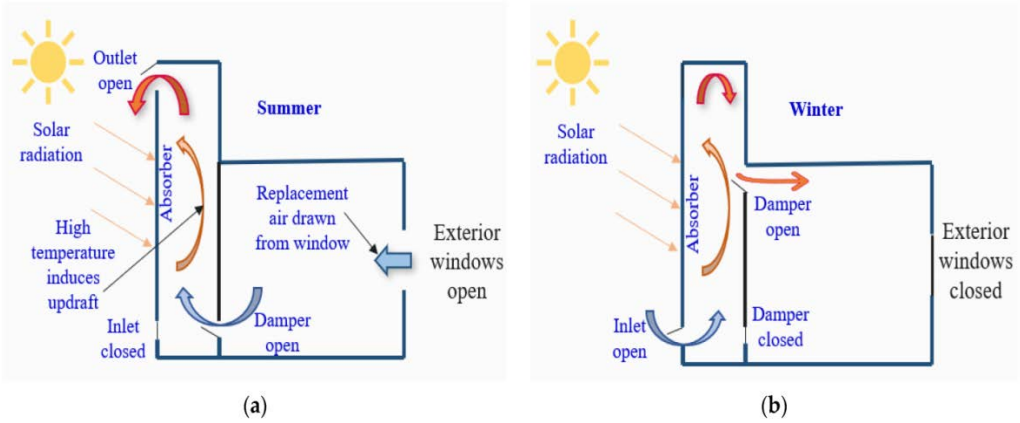

Figure 17: Schematic of solar chimney under heating and cooling modes: (a) cooling mode; (b) heating mode **[22]**

I.8.1.3 Roof Solar Chimney

Practically, there is no significant difference between the two structures except for the position of the wall or tower (chimney) and the absorber, the absorber in a solar chimney maximizes the thermal energy generated by the sun, resulting in a significant temperature difference between the building's interior and exterior, thereby creating a temperature gradient between the air inside the chimney channel and the air at the entrance to the solar chimney, thus forcing cooler air to be pulled from the next room and hot air to be ejected out of the chimney. The solar chimney facilitates natural ventilation in the space by repeating this process **[19]**.

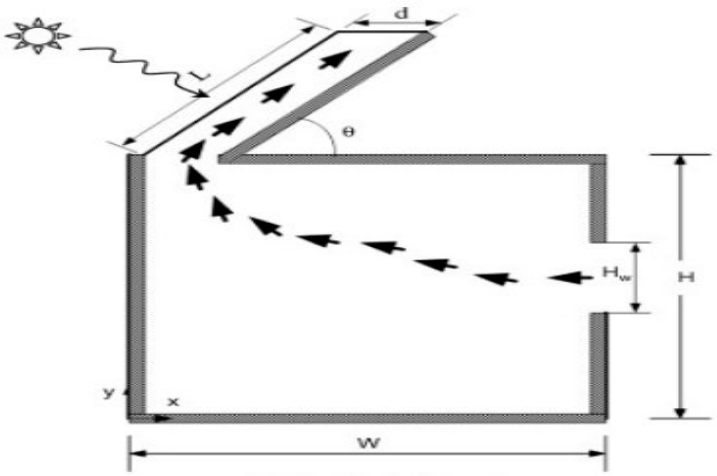

Figure 18: Schematic diagram of roof solar chimney **[23]**

I.8.2 Non-Conventional types

I.8.2.1 Floating solar chimney

The floating solar chimney power generating station, named by the author as Solar Aero-Electric power Plant (SAEP) **[24]**, because it is similar to the hydroelectric generating station, it is economically low cost competitive alternative than the regular concrete solar chimney. It has structurally the same main components as the typical SCPP's that differ in the central section of the chimney (the cylinder) made of a connected balloon-rings of a light tall durable fabric **[25],** as in figure(19); it is flexible and mobile and moves with external wind currents.

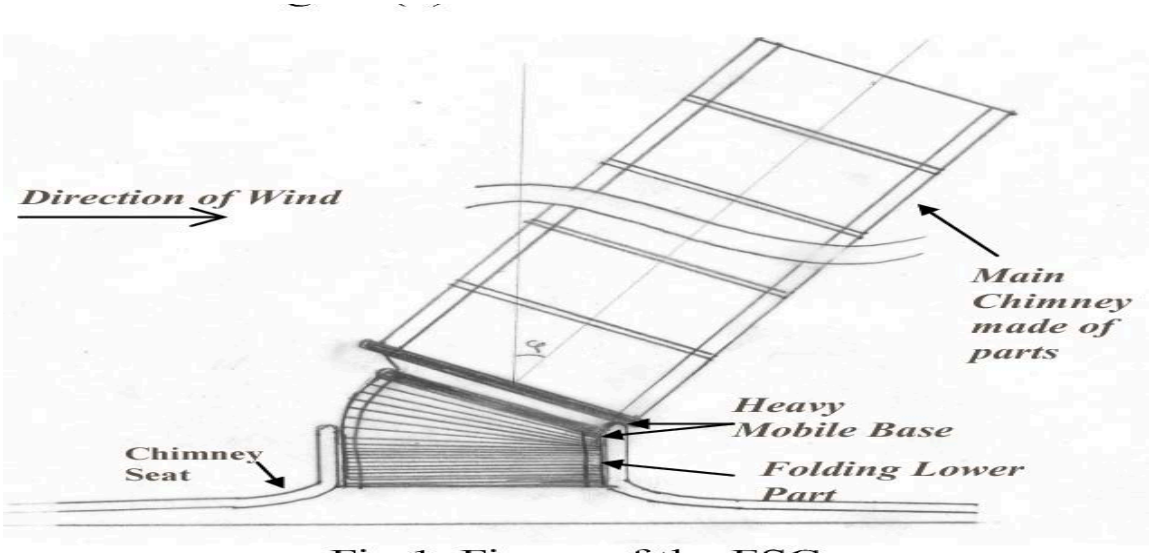

Figure 19: Floating solar chimney diagram **[24]**

I.8.2.2 Sloped solar chimney

The idea of the system was offered by Bilgen et al, the primary idea was to construct a chimney with a collector in a slopped unit. Later it was suggested by Pance et al that the inclined face of the mountain acted as a chimney in addition to the collector. A new study has suggested by Zhou et al. that a hole could be created at the center of a mountain to generate electricity for homes and businesses The collector area was constructed around a mountain in order to produce more power **[26]**.

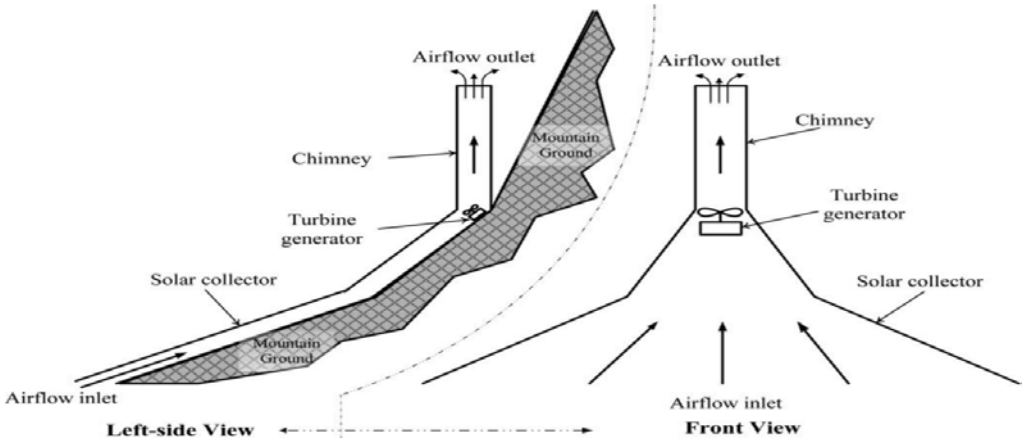

Figure 20: Schematic diagram of a slopped solar chimney **[27]**

I.8.2.3 Geothermal solar chimney

This concept enables adequate electrical power to be delivered even in the absence of sunshine or when meteorological circumstances, such as clouds, obstruct the flow of sunlight, by combining hybrid system of geothermal and solar energy. The system's operating premise is as follows; the ambient air enters the system and flows over the radiators, cooling the condenser water as it passes. The warm air then travels beneath the glass ceiling to gain further heat. The air travels to the system center, where it is guided by several guiding vanes towards the wind turbines, turbines, these last get driven to generate electricity **[26]**.

I.9 Projects and prototypes

I.9.1 Manzanares prototype

The first ever solar thermal project built and constructed in Spain exactly in southern Madrid Manzanares by the German partners Schlaich and Bergermann in 1981 supported and funded by the Spanish government and the German ministry of research and technology , until it was out of service in 1989 **[26]**.

Electrical efficiency at the Manzanares plant was 0.53%, but Schlaich predicts it can be raised to 1.3%. The Manzanares plant's capacity factor was 10% on a big scale, but a 200 MW unit could raise it to 29%.

Details of the construction process:

- Peak power of 50 MW
- 194,6 m height
- Collector radius of 122m
- A single vertical axis single-rotor turbine configuration with four blades installed at the SC base.
- Greenhouse area 6,000 m² of glass cover and 40,000 m² of transparent plastic cover.

Figure 21: Manzanares SCPP **[26]**

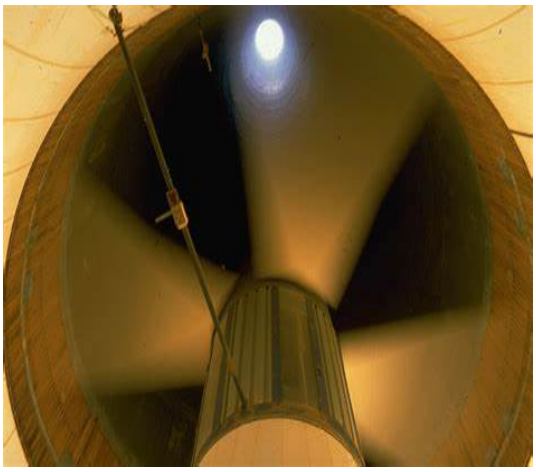

Figure 22: Manzanares SCPP turbins **[28]**

I.9.2 Project of Buronga

In 2001, the Australia government voted in support of the construction of a 200 MW SCPP in Buronga, north of Mildura, Australia. EnviroMission was given the exclusive licence for Solar Tower Technology in order to promote the construction of SCPP in the area. It was suggested that the plant have 1000 m height and 120 m chimney diameter and 7000 m collector diameter **[29]**.

Details of the Project

- 1000 m height
- 7000m collector radius
- Peak power of 200MW

- The investment cost is around 400 million euros.
- Heated air temperature 70 degree Celsius
- Nominal power of the turbines 6.25 MW

Figure 23: Buronga prototype **[30]**

I.9.3 China's Project

In order to enhance the tourism in china a project of hybrid system of wind power and Solar energy power plant of 200 that can supply 400,000 kWh of electricity per year, was co-designed and developed by the University of Science and Technology of Inner Mongolia (IMUST) and the Polytechnic University of Madrid in Spain. **[29]**

It was first constructed in May 2009 in three stages, bringing the total 277 hectares and a total capacity of 27.5 MW, scheduled to be completed in 2013. The power generated by the plant would then be fed into the Inner Mongolian power grid.

Figure 24: China' SCPP prototype **[31]**

I.9.4 Namibien Project

Named ‘the Green tower’, a project of 400 MW SCPP and 1500 m high and 280 m in diameter, and a 37 km2 collector was constructed in Namibia. The collector is also intended to be used in agriculture as a greenhouse where income crops may be cultivated **[32]**.

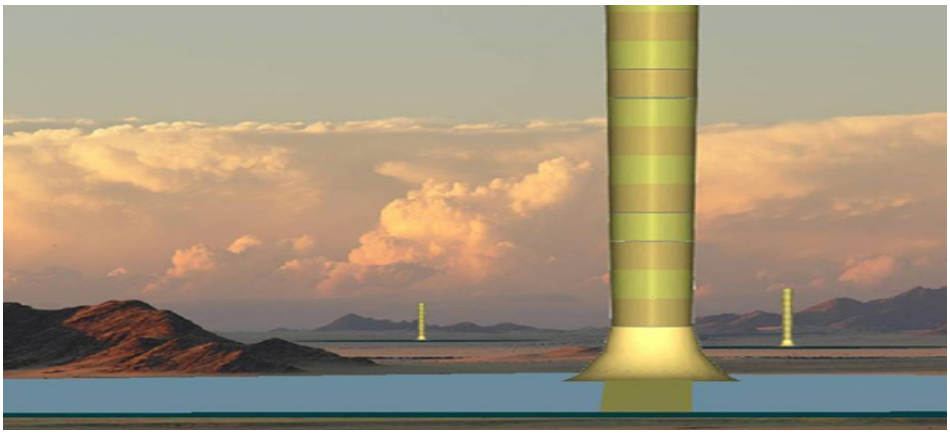

Figure 25: The Namibian SCPP project **[32]**

I.9.5 Egyptian Aswan Project

Aswan has approved the concept of installing solar chimneys since 2012. On February 14, 2018 in the faculty of energy engineering at Aswan university, a project of 300 W per day SCPP was finally put into action. Therefore, everything about the industry aside from the generator is Egyptian **[32]**.

- The solar complex is about 5.1 meters higher than Earth and has a surface area of 28 square meters.
- The chimney is 20 meters in length.
- The chimney cost 250 thousand pounds in total.

Figure 26: Aswan's SCPP **[32]**

I.10 Literature review

The purpose of a study done by **Boualleg Salim, M**. **[33],** is to analyses the energy performance of a solar chimney power plant using several mathematical models. The validation of the results acquired from these several theoretical models by comparison with the practical ones of the Mansanares prototype allows for improved prediction of the performance of the updraft solar chimney power plant.

At the University of Tehran, an analytical and numerical research made by **Alibakhsh Kasaeian et al. [34],** for geometrical optimization of a solar chimney prototype was successfully performed. A basic mathematical model describing the flow was provided. The performance of a solar chimney was evaluated using functional and geometric configurations. The computational predictions were confirmed by comparing them to the experimental data from the solar chimney pilot, which had a height of 2 m and a collector radius of 3 m. Owing to results suggests that a collector entrance of 6 cm, a chimney height of 3 m, and a chimney diameter of 10 cm were the optimum options for the solar chimney pilot that was built. It was discovered that the velocity magnitude may be increased by 4-25% in different conditions; also, the study revealed that the height and diameter of the chimney are the most essential physical elements for solar chimney design.

Toufik Chergui et al. **[35]**, have presented work analyses of heat transmission and airflow in solar chimneys based on several significant characteristics. This research includes a typical instance of application. It entails studying a natural laminar convective heat transfer problem occurring in a chimney. Heat transport and fluid dynamics of airflow are therefore investigated using an axis symmetric system in dimensionless form with well specified boundary conditions. The temperature distribution and velocity field in the chimney and collector are calculated by solving the energy equation and the Navier-Stokes equations using the finite volume approach. The Vahl Davis benchmark solution is used to validate the numerical code based on this modeling.

Davood Toghraie et al. [36], the effects of geometrical parameters on a solar chimney were quantitatively studied in this work using the turbulence model $\kappa-\varepsilon$, inside a solar chimney power plant, continuity, momentum, and energy equations are solved using a 3D finite volume technique. Collector radius, collector height, chimney height, chimney radius, and heat flux were all involved. Changes in these factors were studied for their impact on temperature, velocity, pressure distributions, efficiency, and output power. According to the findings, output power and solar chimney efficiency have positive connections with chimney

height and collector radius, but a negative relationship with collector height. Furthermore, it was discovered that the chimney radius has an ideal range with the highest values for efficiency and output power.

Akchiche Zineb et al. [37] provided a method for ventilation and natural cooling for hot areas in this study. A solar chimney creates airflow through the enclosure. To forecast the behavior of the chimney, an experimental setup was created, followed by a simulation using the fluent software for a solar chimney with different shapes and two inclinations. To anticipate the ventilation rate, an application is operating on a piece of size (1m x 1m x 1m) equipped with a solar chimney inclined 45 degrees to the horizontal integrated over the upper section. to increase ventilation quality and reduce electricity usage while maintaining thermal comfort, an air-ground was introduced. They were able to create an air/ground design because to the drop in temperature at the room's entry, and they came to the conclusion that

- The mechanism becomes more efficient as solar radiation levels grow.
- The amount of air flow is significantly determined by the size of the chimney.
- A 45-degree angle from horizontal corresponds to the best heat circulation.
- The amount of solar radiation affects the temperature and air flow at the chimney's exit.

Arkan Kh. Al-Taie & Ali Hayder Mutib [38], provided a numerical simulation to examine the effectiveness of a solar chimney power station. FLUENT software was used to model and analyse the solar chimney power station at a small scale system in order to solve the governing equations of conservation of mass, momentum, energy, Do-intensity, k, and equations. The glass roof collector, chimney (tower), and wind turbine are the three key components of solar chimney power plants. The input velocity to the wind turbine determines the system's output power. The collector-chimney connection type affects the turbine inlet velocity. The findings shown that performance characteristics, particularly air flow velocity, are influenced by the shape of the entry region (collector-chimney junction type). When compared to using a straight connection, using a curved or rounded junction with a deflector will increase system mass flow rate by 37.65%.

According to **Emad Abdelsalam et al. [39]**, the present effort involves an updated version of the Classic Solar Chimney Power Station's construction known as the Solar Double Chimney Power Plant (SDCPP) (SCPP). In order to increase power output, the SCPP design has been changed by the addition of a co-centric secondary exterior chimney to the SCPP structure 10 cooling towers (CT) with water sprayers and turbines for additional power generation ensure proper functioning (day and night). Using MATLAB, a mathematical

model that incorporates the system's mass equations and energy balance was created. The new design's material combination produced a thermal efficiency of 1.6%, which is 200 times more than SCPP. The local cost of energy (LCOE) for the new system was 50% lower than for the conventional SCPP, according to the economic analysis.

Rashid, F. L., & Alnomani, S.N [40], provide a numerical analysis utilizing the K-model in the CFD application FLUENT, of a solar chimney with a conical collector that has particular dimensions. To study the impact of the spiral's square cross section on the distribution of air velocity, it was attached to the collector.

Arkan k. Al-Taaie et al. [41], developed a sloping solar chimney system and performed measures of the solar chimney power plant in Baghdad, Iraq using Fluent the governing equations for incompressible, three-dimensional, stable, turbulent standard $\kappa-\varepsilon$ with boussinesq approximation have been solved, in addition to the continuity, Navier-stocks, energy, and radiation transfer equations. Considering the radiation intensity and collector angle conditions (0°, 15°, and 30°).Results show that as the collector angle rises, the velocity rises as well, peaking at a collector angle of 30°, around periods of increased sun intensity (7:30,8:15,9,10 AM), the temperature rises with the angle of the collector tile, but falls at 12:30 PM. The study shows that Iraqi weather is suitable for this system.

The project of **Gahgah, M [42]**, includes simulating flows in solar chimneys numerically. The method of mathematical modeling employed is based on flows in a two-part, opened enclosure, consisting of a cylinder and a disc To model air flow in a chimney while accounting for different flow regimes(laminar and turbulent flows), this study entails creating computer software with dimensionless variables and generalized coordinates, utilizing the finite volume technique with suitable boundary conditions occurring in a complicated geometry with dimensionless variables, such as a solar chimney power plant. This work is a keystone in comprehending the thermo-fluid aspect analysis of solar chimney efficiency that occurs in solar chimney power plants and under steady state parameters.

CHAPTER II

MODELING AND PROBLEM FORMULATION

II.1 Introduction

The physical problem is presented in this chapter using partial differential equations (PDE) system that governs the phenomenon of natural convection inside the physical domain represented by a solar chimney in the cylindrical coordinates.

II.2 Problem description

A study of two dimensional air flow caused by natural convection within the solar chimney represented in figure (1), taking in consideration the appropriate assumptions and the mathematical formalisms using the Boussinesq approximation.

Taking into account that the exterior walls are regarded isothermal and kept at a constant ambient temperature T_c, while the soil that represents the ground wall is considered isothermal with T_h, with $T_h > T_c$.

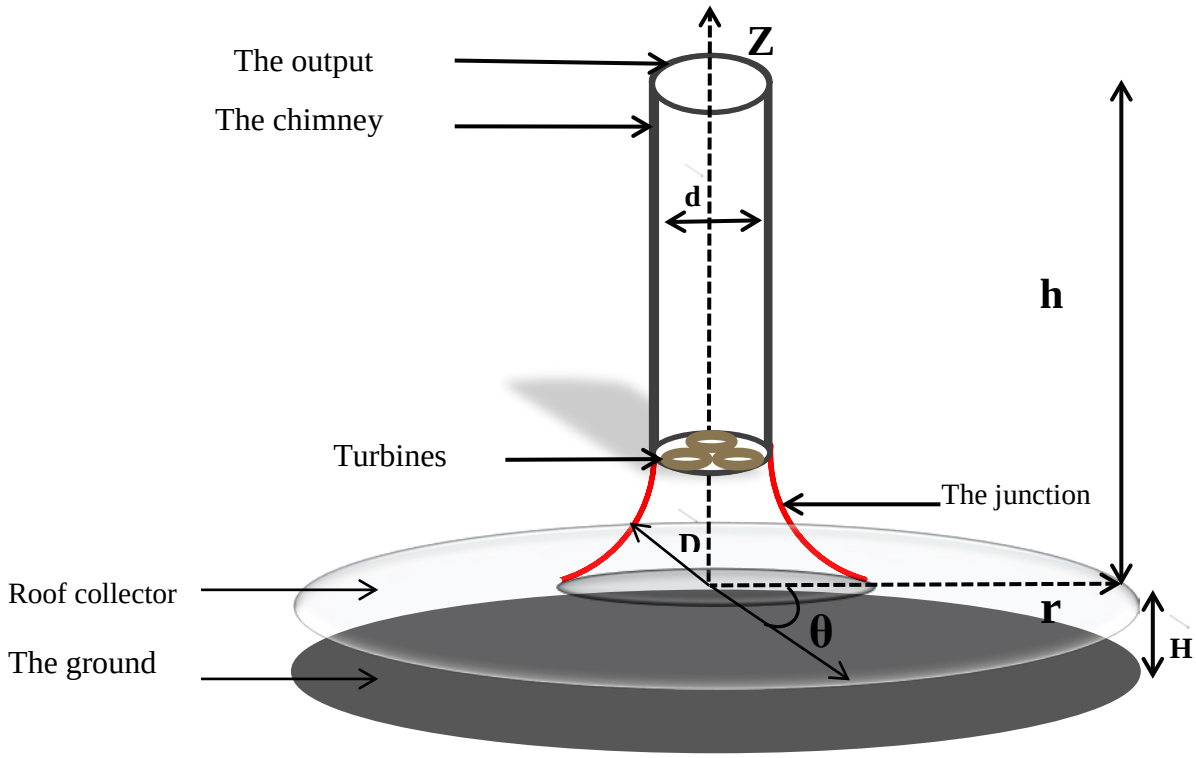

Figure 1: Geometry of a solar chimney with a curved junction.

II.3 Mathematical formulation

Mathematical formalisms appropriate for the geometry and flow regime are used to define the problem:

- **Continuity equation**

$$\frac{\partial \rho}{\partial t} + \text{div}(\rho.\vec{v}) = 0 \quad \text{(II.1)}$$

Where:

ρ: Density of the fluid

$\vec{v}$: Velocity component

- **Momentum conservation equations:**

$$\rho\left(\frac{\partial \vec{v}}{\partial t} + \left(\vec{v}.\overrightarrow{\text{grad}v}\right)\right) = -\vec{\nabla}p + \rho\vec{g} + \mu\Delta\vec{k} \quad \text{(II.2)}$$

- **Energy equation:**

$$\frac{\partial T}{\partial t} + \left(\vec{v}.\overrightarrow{\text{grad}\,T}\right) = \frac{\lambda}{\rho Cp}\Delta T \quad \text{(II.3)}$$

II.4 Simplifying hypothesis

- The flow is assumed to be bidimensional, permanent, and laminar.
- The fluid is assumed to be Newtonian and incompressible.
- The flow is assumed to be axisymmetric where$\left(\frac{\partial}{\partial \theta}\right) = 0$.
- The conduction and the radiation through the collector are neglected.
- Viscous dissipation and pressure forces are neglected in the energy equation.
- The Boussinesq approximation is used for the variations of the density in the terms of force of volume and directly correlated with temperature T. The reference temperature T_0 controls the fluid's physical characteristics, which are constant in the other terms of the equations;

$$\rho = \rho_0\,(1 - \beta_T\,(T - T_0)) \quad \text{(II.4)}$$

Where:

$\beta_T = -\frac{1}{\rho_0}\frac{\partial P}{\partial T}$: The coefficient of thermal expansion

II.5 Mathematical modeling in cylindrical coordinates

The general governing equations are defined in the cylindrical coordinates (r, θ, z) as follows:

- **Continuity equation:**

$$\frac{\partial \rho}{\partial t} + \rho\left(\frac{1}{r}\frac{\partial (r v_r)}{\partial r} + \frac{1}{r}\frac{\partial v_\theta}{\partial \theta} + \frac{\partial v_z}{\partial z}\right) + \left(v_r\frac{\partial \rho}{\partial r} + \frac{v_\theta}{r}\frac{\partial \rho}{\partial \theta} + v_z\frac{\partial \rho}{\partial z}\right) = 0 \quad \text{(II.5)}$$

- **Momentum conservation equations:**

- **In (r-direction):**

$$\rho\frac{\partial(v_r)}{\partial t}+v_r\frac{\partial(v_r)}{\partial r}+\frac{(v_\theta)}{r}\frac{\partial(v_\theta)}{\partial\theta}-\frac{(v_\theta)^2}{r}+v_z\frac{\partial v_r}{\partial z}=-\frac{\partial p}{\partial r}+\rho g_r+\mu(\frac{1}{r}\frac{\partial}{\partial r}\left(r\frac{\partial v_r}{\partial r}\right)-\frac{v_r}{r^2}+\frac{1}{r^2}\frac{\partial^2 v_r}{\partial\theta^2}-\frac{2}{r^2}\frac{\partial v_\theta}{\partial\theta}+\frac{\partial^2 v_r}{\partial z^2}) \quad (II.6)$$

- **In (θ- direction):**

$$\rho(\frac{\partial(v_\theta)}{\partial t}+(v_r)\frac{\partial(v_\theta)}{\partial r}+\frac{(v_\theta)}{r}\frac{\partial(v_\theta)}{\partial\theta}+\frac{v_\theta v_r}{r}+v_z\frac{\partial v_\theta}{\partial z}=$$
$$-\frac{1}{r}\frac{\partial p}{\partial\theta}+\rho g_\theta+\mu(\frac{1}{r}\frac{\partial}{\partial r}\left(r\frac{\partial v_\theta}{\partial r}\right)-\frac{v_\theta}{r^2}+\frac{1}{r^2}\frac{\partial^2(v_\theta)}{\partial\theta^2}-\frac{2}{r^2}\frac{\partial v_r}{\partial\theta}+\frac{\partial^2 v_z}{\partial z^2}) \quad (II.7)$$

- **In(z -direction)**

$$\rho(\frac{\partial(v_z)}{\partial t}+v_r\frac{\partial(v_z)}{\partial r}+\frac{v_\theta}{r}\frac{\partial v_z}{\partial\theta}+v_z\frac{\partial v_z}{\partial z})=-\frac{\partial p}{\partial z}+\rho g_z+\mu(\frac{1}{r}\frac{\partial}{\partial r}\left(r\frac{\partial v_z}{\partial r}\right)+\frac{1}{r^2}\frac{\partial^2 v_z}{\partial\theta^2}+\frac{\partial^2 v_z}{\partial z^2}) \quad (II.8)$$

❖ **Energy equation:**

$$\frac{\partial T}{\partial t}+v_r\frac{\partial T}{\partial r}+\frac{v_\theta}{r}\frac{\partial T}{\partial\theta}+v_z\frac{\partial T}{\partial z}=\frac{\lambda}{\rho c_p}\left(\frac{1}{r}\frac{\partial}{\partial r}\left(r\frac{\partial T}{\partial r}\right)+\frac{1}{r^2}\frac{\partial^2 T}{\partial\theta^2}+\frac{\partial^2 T}{\partial z^2}\right) \quad (II.9)$$

According to the hypothesis we mentioned before, the continuity, momentum, and energy balance equations are reformulated as follows:

❖ **Continuity equation:**

$$\frac{1}{r}\frac{\partial(rv_r)}{\partial r}+\frac{\partial v_z}{\partial z}=0 \quad (II.10)$$

❖ **Momentum conservation equations:**

$$\rho\left(v_r\frac{\partial v_r}{\partial r}+v_z\frac{\partial v_r}{\partial z}\right)=-\frac{\partial p}{\partial r}+\mu\left(\frac{1}{r}\frac{\partial}{\partial r}\frac{\partial(rv_r)}{\partial r}-\frac{v_r}{r^2}+\frac{\partial^2 v_r}{\partial z^2}\right) \quad (II.11)$$

$$\rho\left(v_r\frac{\partial v_z}{\partial r}+v_z\frac{\partial v_z}{\partial z}\right)=-\frac{\partial p}{\partial z}+g_z\rho\beta_T(T-T_0)+\mu\left(\frac{1}{r}\frac{\partial}{\partial r}\frac{\partial(rv_z)}{\partial r}+\frac{\partial^2 v_z}{\partial z^2}\right) \quad (II.12)$$

❖ **Energy equation:**

$$v_r\frac{\partial T}{\partial r}+v_z\frac{\partial T}{\partial z}=\frac{\lambda}{\rho c_p}\left(\frac{1}{r}\frac{\partial}{\partial r}\left(r\frac{\partial T}{\partial r}\right)+\frac{\partial^2 T}{\partial z^2}\right) \quad (II.13)$$

II.6 Boundary conditions

The boundary conditions are summarized as following:

- At the air input: $T = T_c$, $v_r = 0$, $v_z = 0$
- At the output: $\frac{\partial v_z}{\partial z} = \frac{\partial (v_r)}{\partial z} = \frac{\partial (T)}{\partial z} = 0$
- Boundary Conditions for the ground: $T_{ground} = T_h$, $v_r = 0$, $v_z = 0$
- Boundary Conditions for the collector: $T = T_c$, $v_r = 0$, $v_z = 0$

II.7 Dimensionless mathematical model

It is necessary to acquire the non-dimension version of the modeling equations that we create based on the following typical quantities:

$$r^+ = \frac{r}{D} \ , z^+ = \frac{z}{D}, T^+ = \frac{T - T_c}{T_h - T_c} \ , P^+ = \frac{P}{\rho(\alpha/D)^2}$$

$$v_r^+ = \frac{v_r}{(\alpha/D)} \ , v_z^+ = \frac{v_z}{(\alpha/D)}$$

- **Continuity equation:**

$$\frac{1}{r^+}\frac{\partial (r^+ v_r{}^+)}{\partial r^+} + \frac{\partial v_z{}^+}{\partial z^+} = 0 \qquad \text{(II.14)}$$

- **Momentum conservation equations:**

$$v_r{}^+ \frac{\partial v_r^+}{\partial r^+} + v_z{}^+ \frac{\partial v_r^+}{\partial z^+} = -\frac{\partial p^+}{\partial r^+} + P_r \left(\frac{1}{r^+}\frac{\partial}{\partial r^+}\frac{\partial (r^+ v_r{}^+)}{\partial r^+} - \frac{v_r{}^+}{r^{+2}} + \frac{\partial^2 v_r{}^+}{\partial z^{+2}} \right) \qquad \text{(II.15)}$$

$$v_r{}^+ \frac{\partial v_z^+}{\partial r^+} + v_z{}^+ \frac{\partial v_z^+}{\partial z^+} = -\frac{\partial p^+}{\partial z^+} + P_r \left(\frac{1}{r^+}\frac{\partial}{\partial r^+}\frac{\partial (r^+ v_z{}^+)}{\partial r^+} + \frac{\partial^2 v_z{}^+}{\partial z^{+2}} \right) + R_a \cdot P_r \cdot T^+ \qquad \text{(II.16)}$$

- **Energy equation:**

$$v_r{}^+ \frac{\partial T^+}{\partial r^+} + v_z{}^+ \frac{\partial T^+}{\partial z^+} = \frac{1}{r^+}\frac{\partial T^+}{\partial r^+} + \frac{\partial^2 T^+}{\partial r^{+2}} + \frac{\partial^2 T^+}{\partial z^{+2}} \qquad \text{(II.17)}$$

II. 8 Dimensionless boundary condition

- At the air input: $T^+ = 0$, $v_r^+ = 0$, $v_z^+ = 0$
-
- At the output: $\frac{\partial v_z{}^+}{\partial z^+} = \frac{\partial (v_r)^+}{\partial z^+} = \frac{\partial T^+}{\partial z^+} = 0$
- Boundary Conditions for the ground: $T_h{}^+ = 1$, $v_r^+ = 0$, $v_z^+ = 0$
- Boundary Conditions for the collector: $T_C{}^+ = 0$, $v_r^+ = 0$, $v_z^+ = 0$

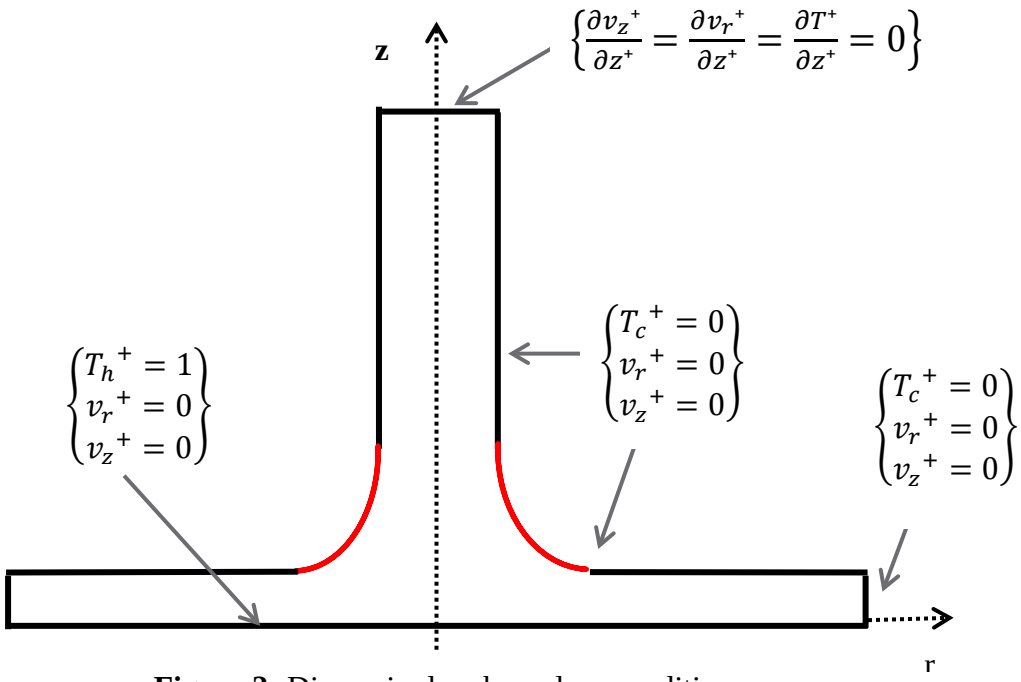

Figure 2: Dimensionless boundary condition

CHAPTER III

NUMERICAL SIMULATION SOFTWARE

III.1. Introduction

Numerical computation technology provides an alternative to physical research and engineering studies which are difficult to implement experimentally, by use of digital simulation software that has been optimized for a computer processor to handle a lot of problems with consideration for the appropriate geometry, physical parameters, and boundary conditions.

In this chapter, a computational fluid dynamics (CFD) analysis model using COMSOL Multiphysics Simulation Software is performed to simulate the natural convection of air within the solar chimney by solving the governed equations system mentioned in the previous chapter.

III.2. COMSOL software overview

Almost all (CFD) software has three primary parts:

- Preprocessor for modeling and meshing.
- Computational processor (solver) using digital methods (the Finite differences method, finite elements method, spectral methods and finite volumes method.
- The postprocessor where the outcomes are provided in a format appropriate for the perception of the problems physics (plot).

COMSOL Multiphysics is one of the CFD's which is numerical computing software using finite element method that allows modeling a wide variety of physical and engineering phenomena characterizing a real problem based on partial differential equations (PDEs) **[43]**.

One of this software's merits is the ability to quickly transform single-physics models into multiphysics models that simultaneously handle related physics problems including fluid mechanics, heat transport, electricity, electromagnetic, chemistry, mechanical structures, and so on.

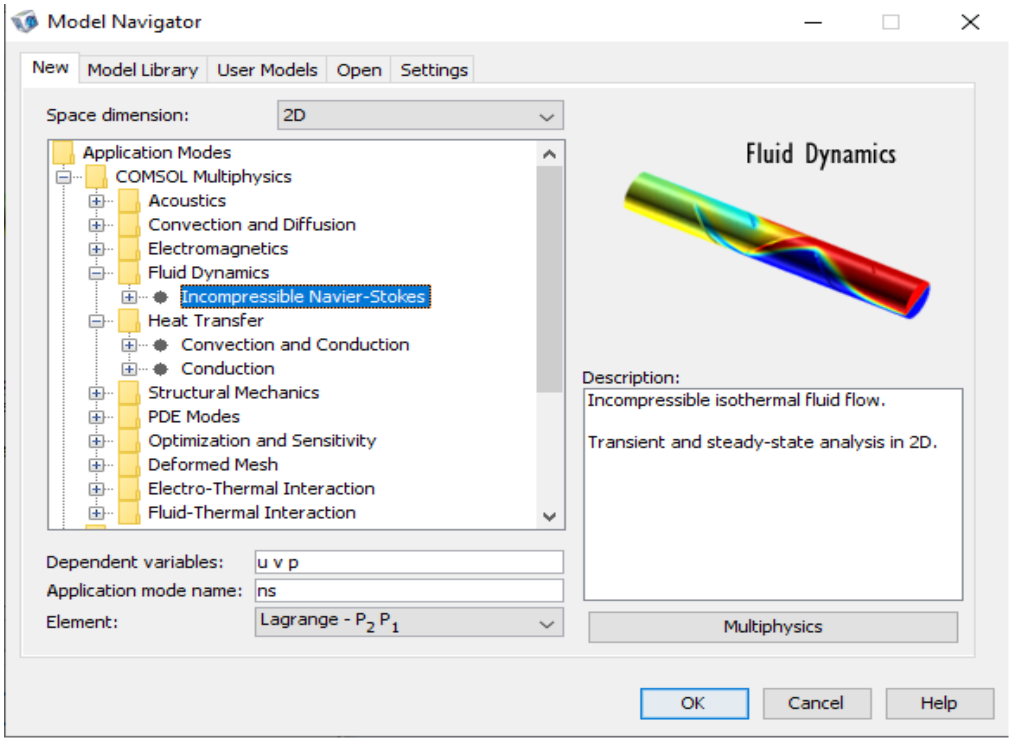

Figure 1: The software interface

III.3. Basic Procedures of COMSOL Simulation

- Application mode selection
- Creating or importing the geometry
- Meshing the geometry
- Defining the physics on the domains and at the boundaries
- Solving the model
- Post processing the solution
- Performing parametric studies

Step1: Choosing the application mode

This step includes selecting the appropriate mode and space dimensions in our case (2D) and the specifying variables from **Multiphysics** then selecting **Model navigator** button, in our case the model tree shows:

- Geom1(2D):
  - Incompressible Navier-Stocks (ns)
  - Convection and Conduction (cc)

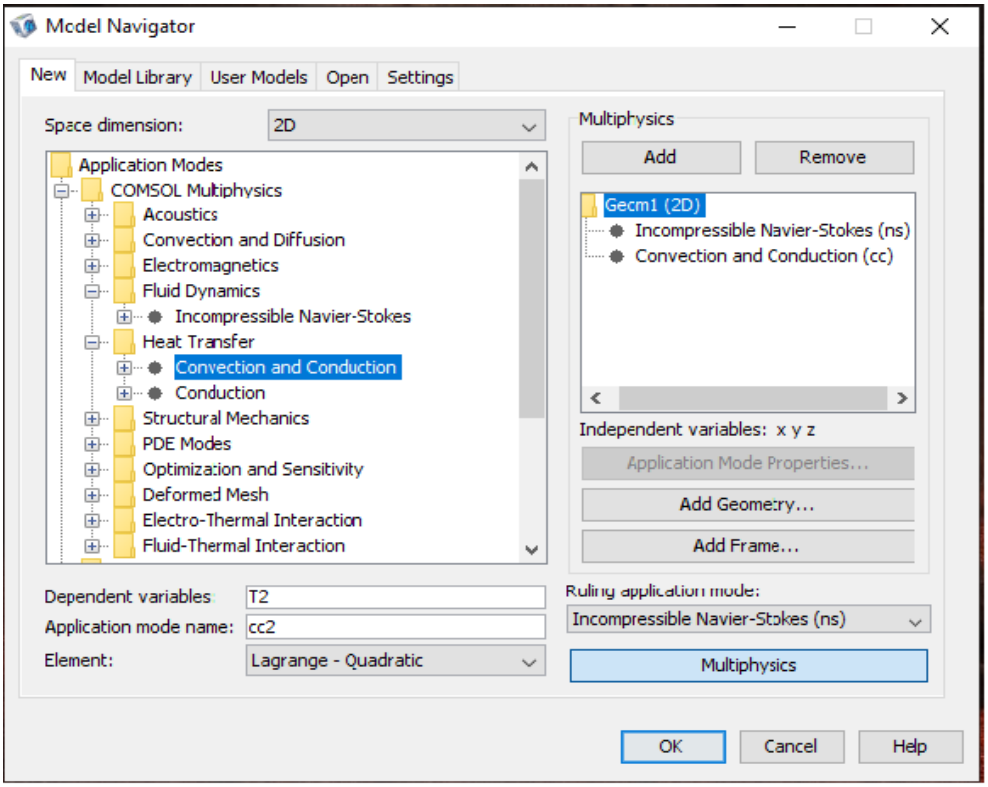

Figure 2: Model navigator window

- **Step 2: Geometry creating**

At this stage, the physical design is performed using the CAD tools on the draw menu, selection points with appropriate coordinates, then connect them with straight lines so it creates the chimney geometry.

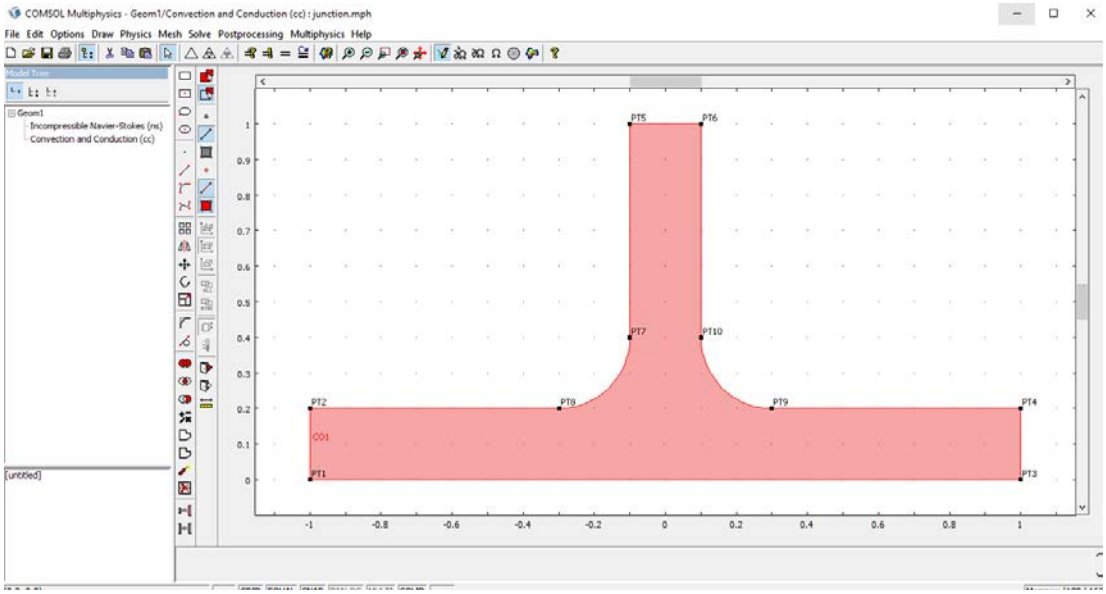

Figure 3: Geometry Creation

- **Step3: Constants input**

By selecting **Options** then **Constants**

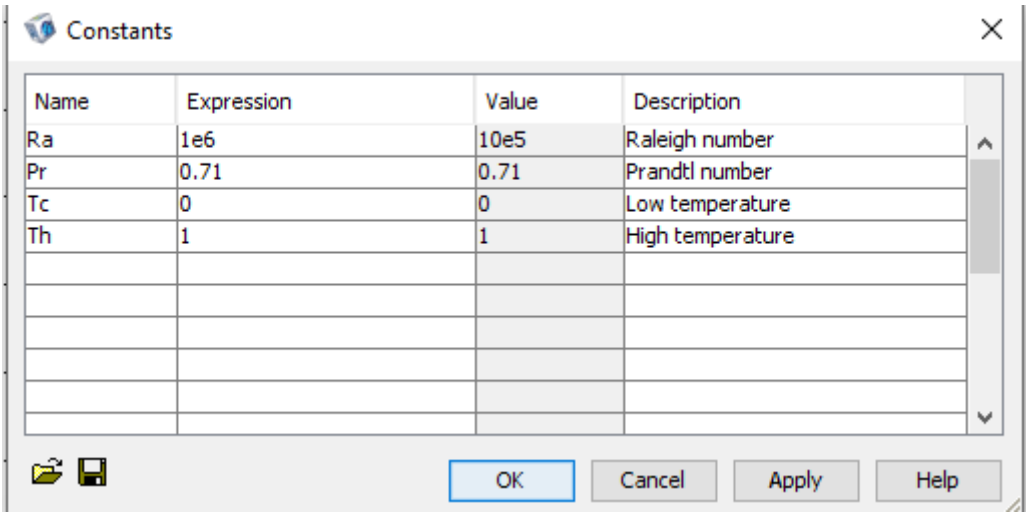

Figure 4: Constants input

- **Step4: Defining the physics**

This step includes defining all the setting and the equation for the physics in the model

- **Physics → Subdomain setting:** select subdomain and then define the fluid properties (in our case it is dimensionless)

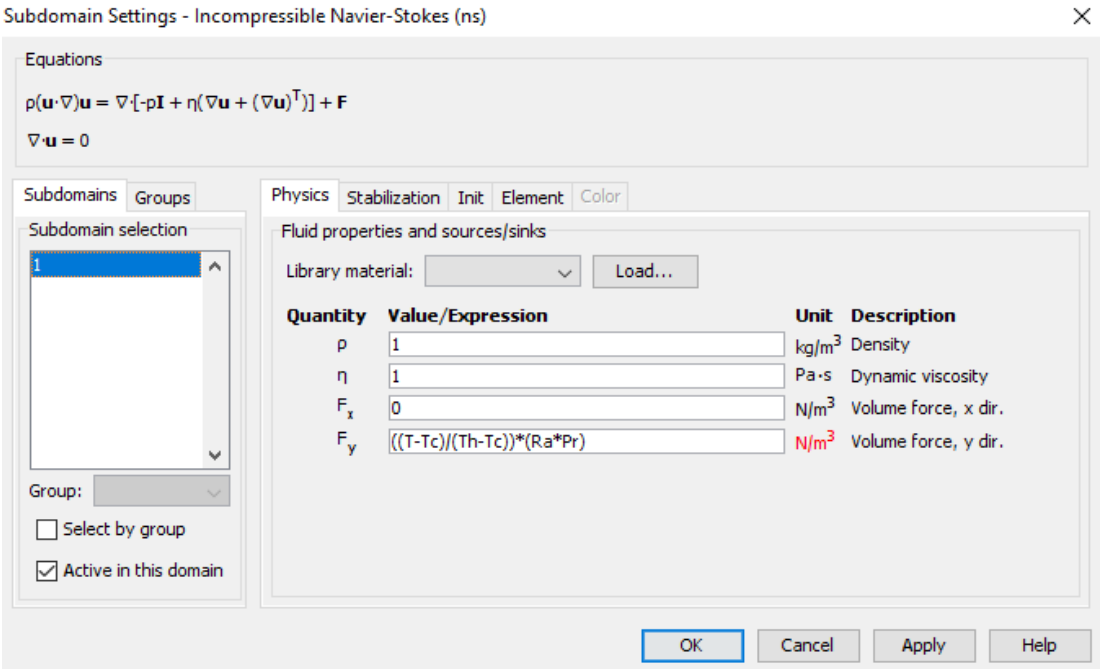

Figure 5: Subdomain setting window in the Navier-stocks mode

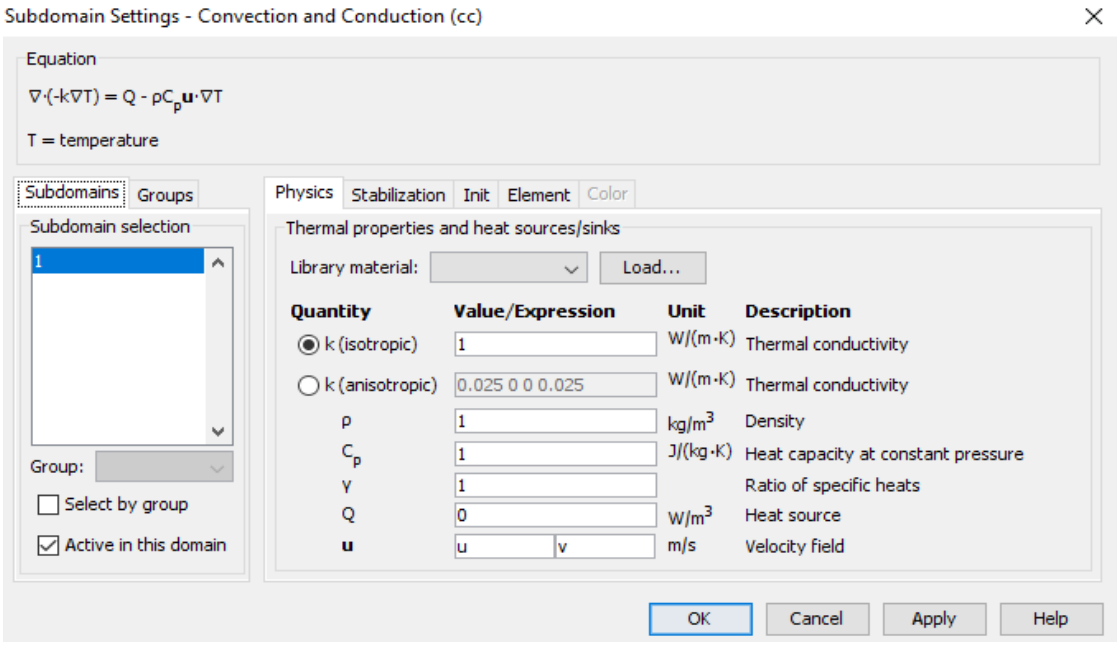

Figure 6: Subdomain setting in the convection and conduction mode

- **Physics → Boundary condition:** the boundary conditions for each border will be defined with the Boundary setting window then confirming the selection.

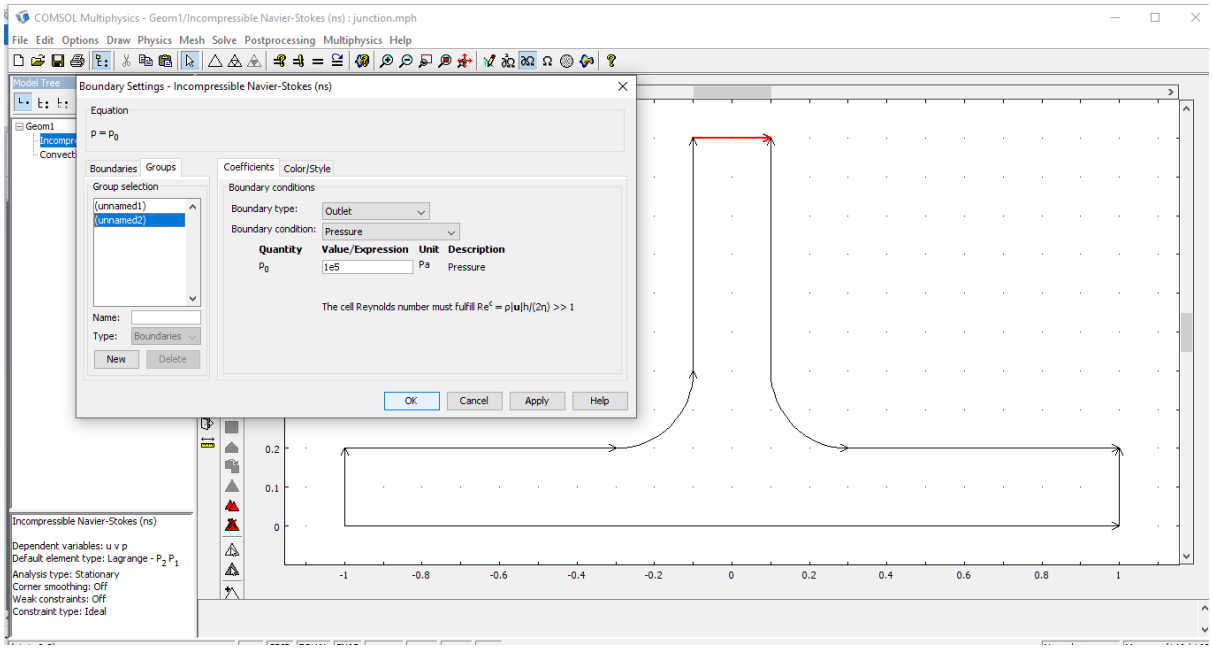

Figure 7: Define the boundary conditions in Incompressible Navier-stokes mode for the outlet

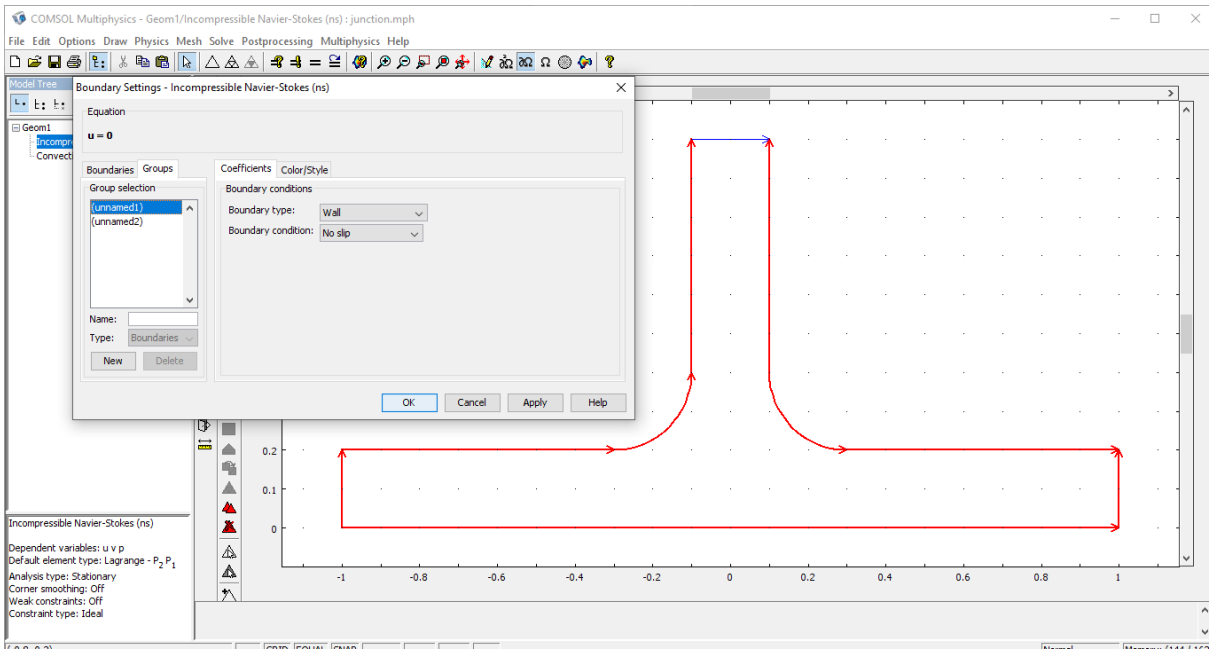

Figure 8: Define the boundary conditions in Incompressible Navier-stokes mode for the walls

- **Step 5: Meshing the geometry**

By selecting the **Mesh** in the tool bar then **initialize mesh** then **refine mesh** then **refine selection.**

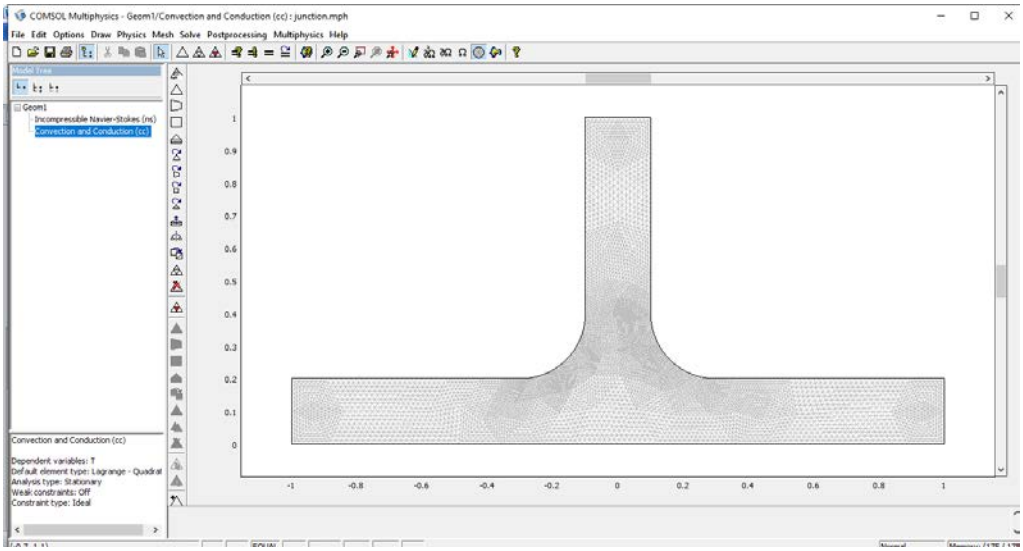

Figure 9: Refined mesh window

- **Step 6: Solving the model**

We modified certain solver properties in the Solver Parameters menu.

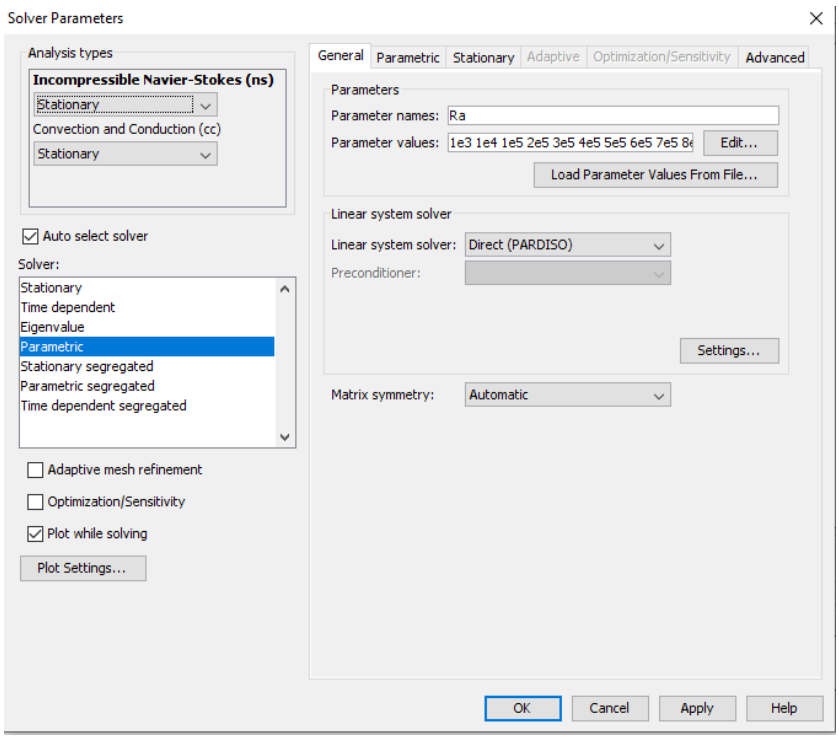

Figure 10: Solver parameters window

- **Step 7: Post processing and plotting**

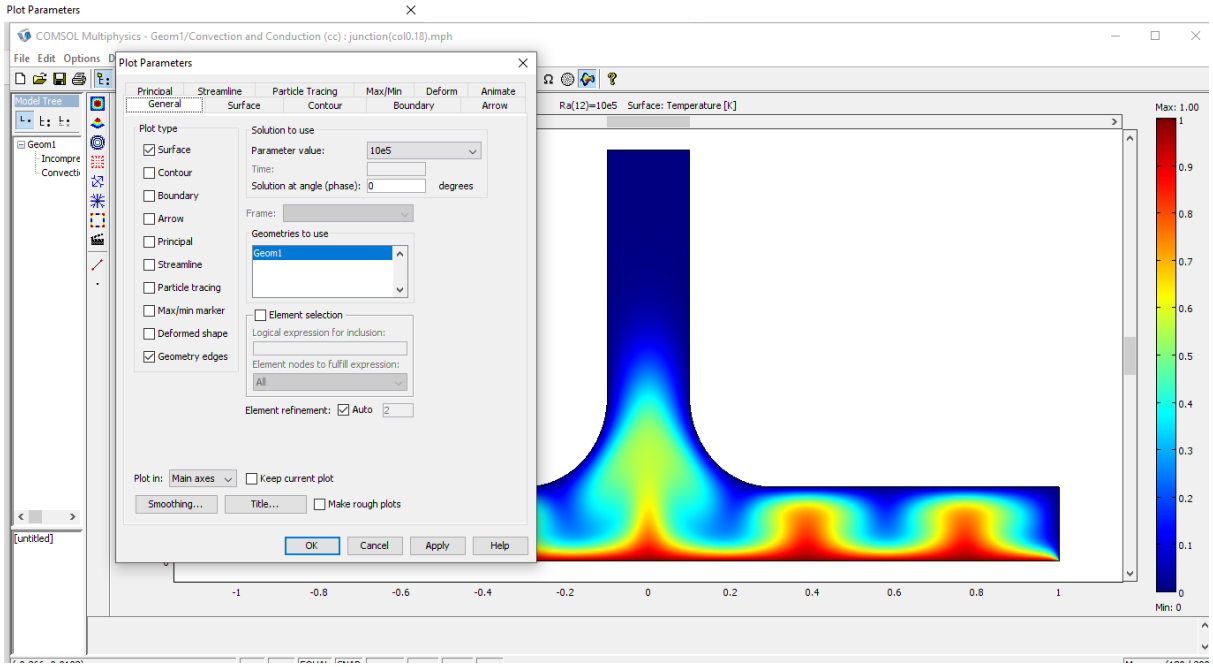

Figure 11: Post processing and outcome visualization

CHAPTER IV

RESULTS AND DISCUSSION

IV.1. Introduction

The study's findings, which relate to Rayleigh's number and the chimney geometric parameters effects on the airflow development within the solar chimney, are presented in this chapter and illustrated in isolines of dimensionless velocity and temperature as well as profiles of the vertical velocity component that acts directly on the turbine to generate power.

IV.2. Effect of Rayleigh number Ra on temperature and velocity isolines

IV.2.1. Curved junction with major radius Rc =0.24

Figures (1-6), represent isotherms and velocity field for three different values of Rayleigh number ($Ra=10^4$, $Ra=5x10^5$ and $Ra=10^6$) respectively. Where figure (1) shows the isotherms for $Ra=10^4$, in this case isotherms are parallel lines all along the collector area and the temperature distribution decreases form the ground where the maximum temperature is located upward to the collector's roof (the cold wall) indicating that the heat transfer in this region is dominated mainly by the pseudo-conduction mode, noticing a slight deformation in the entry region of the chimney that demonstrates the presence of a very weak intensity of natural convection in this instability zone, figure (2) represents velocity field distribution with counter rotating cells at the entry region of the chimney and at the inlet regions of the collector confirming that air motion is very weak to generate the flow.

Figure (3) illustrates isotherms for $Ra=5x10^5$, the figure shows a slight increase in the distortion of the isothermal lines throughout the entire space with an increase of the convection intensity in the chimney's tower entry. This indicates the beginning of the predominance of natural convection mode on the Pseudo-conduction mode which is contributing minimally in the airflow generation. Figure (4) shows two symmetrical counter rotating cells at the chimney's entry mediated by a main cell moving upward representing a significant development of flow field.

Figures (5-6), showing a fully deformed isothermal lines and fully developed velocity field of approximately two times more intense compared to the previous Rayleigh value. We can clearly conclude that the significant increase of Rayleigh value reaching $Ra=10^6$ provides an intensification of air flow where less dense hot air rises toward the cold wall and then start condensing and return back down by gravity illustrated as adjacent convective cells all along the space, this is known as the buoyancy driven flow, thus the heat transfer in the solar chimney is fully dominated by the natural convection mode.

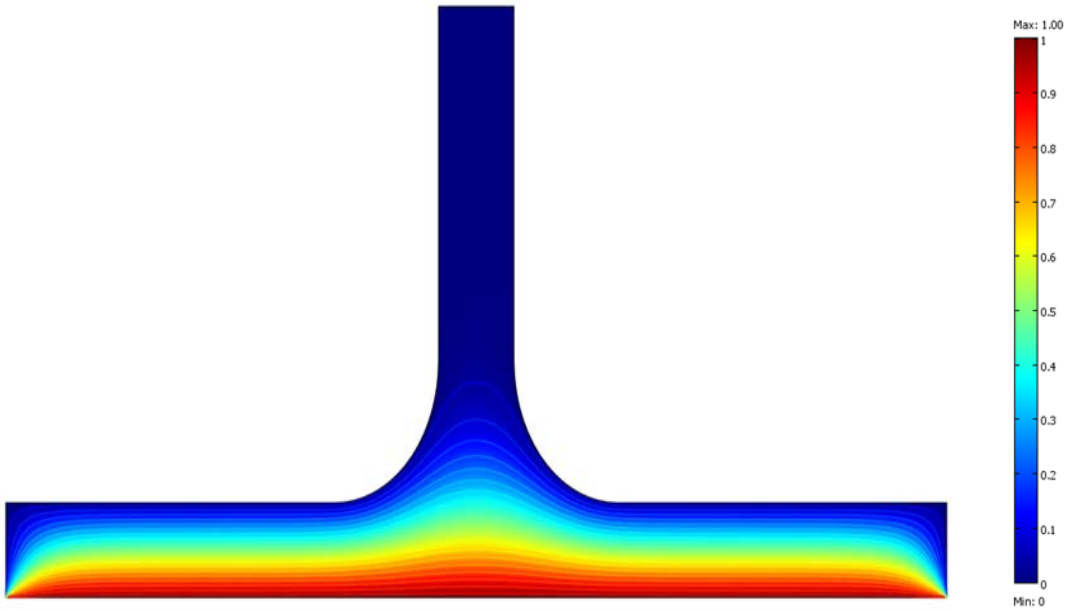

Figure 1: Dimensionless temperature distribution for Rc=0.24 and Ra=10^4

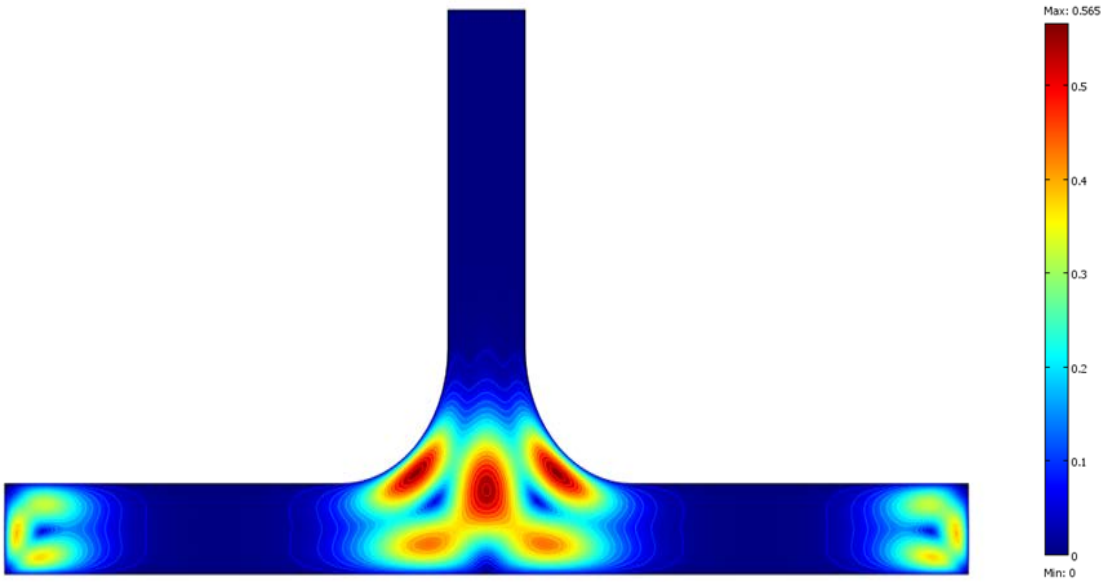

Figure 2: Dimensionless velocity field for Rc=0.24 and Ra=10^4

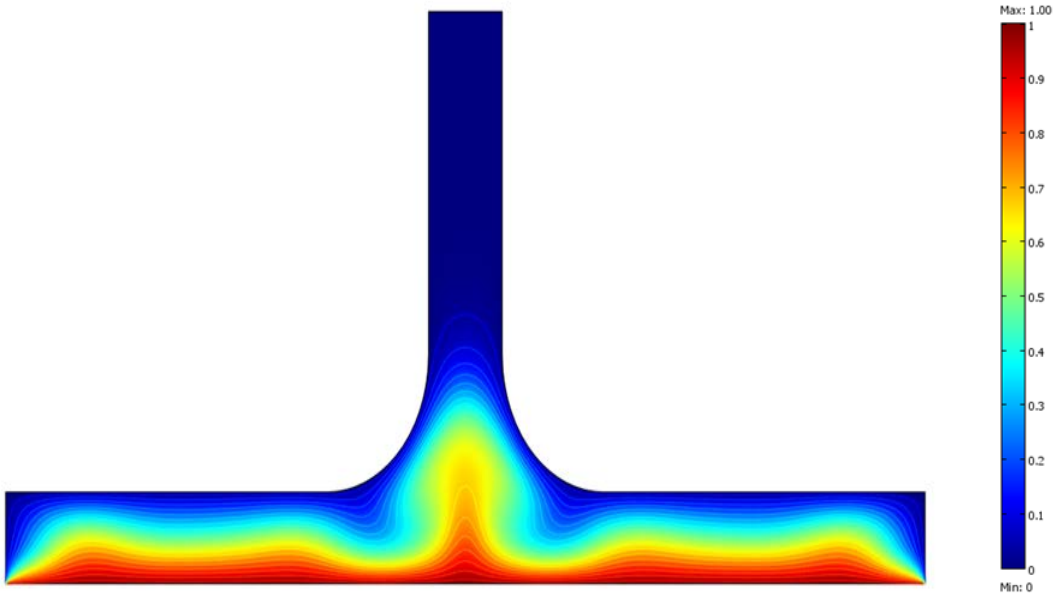

Figure 3: Dimensionless temperature distribution for Rc=0.24 and Ra=5x10^5

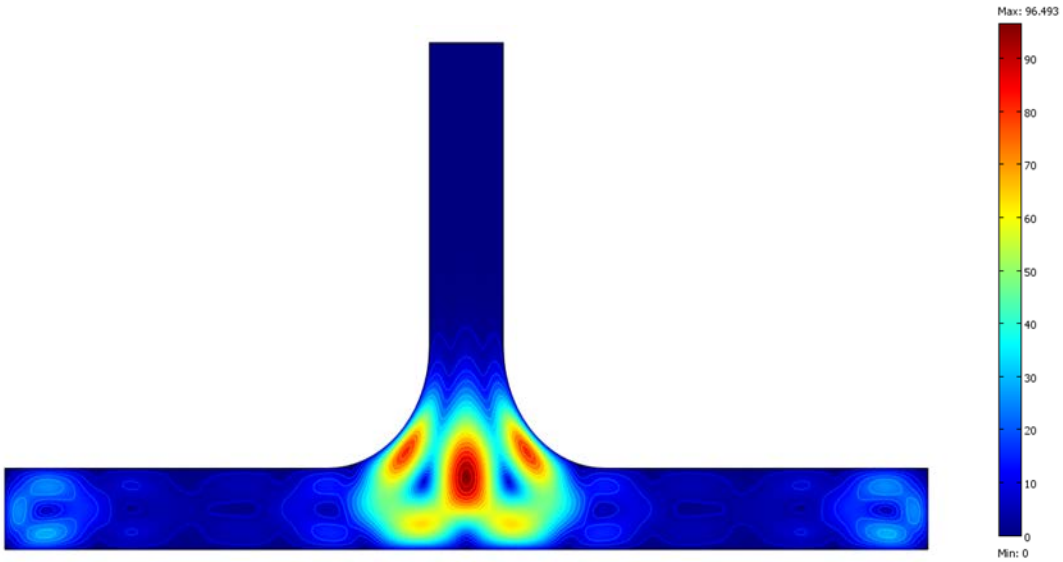

Figure 4: Dimensionless velocity field for Rc=0.24 and Ra=5x10^5

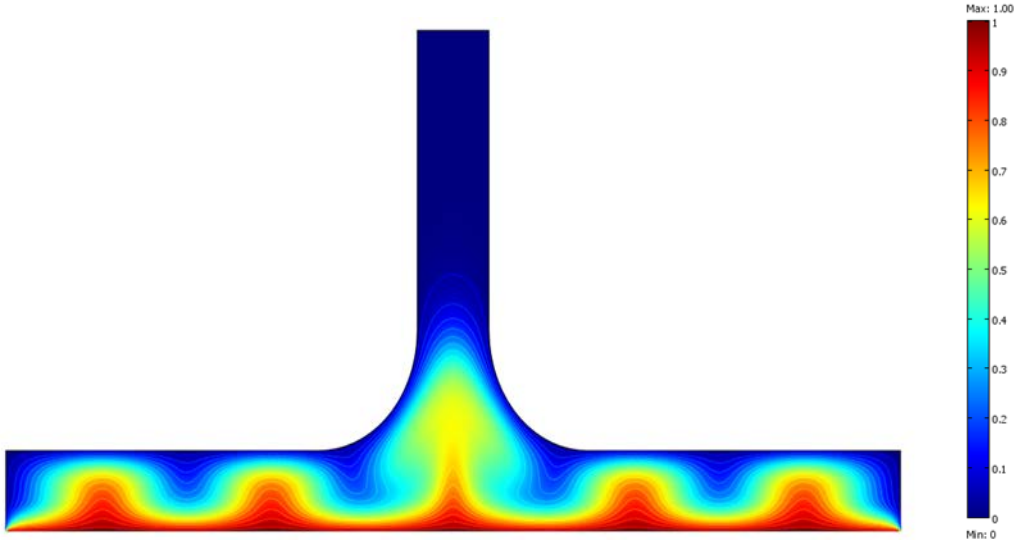

Figure 5: Dimensionless temperature distribution for Rc=0.24 and Ra=10^6

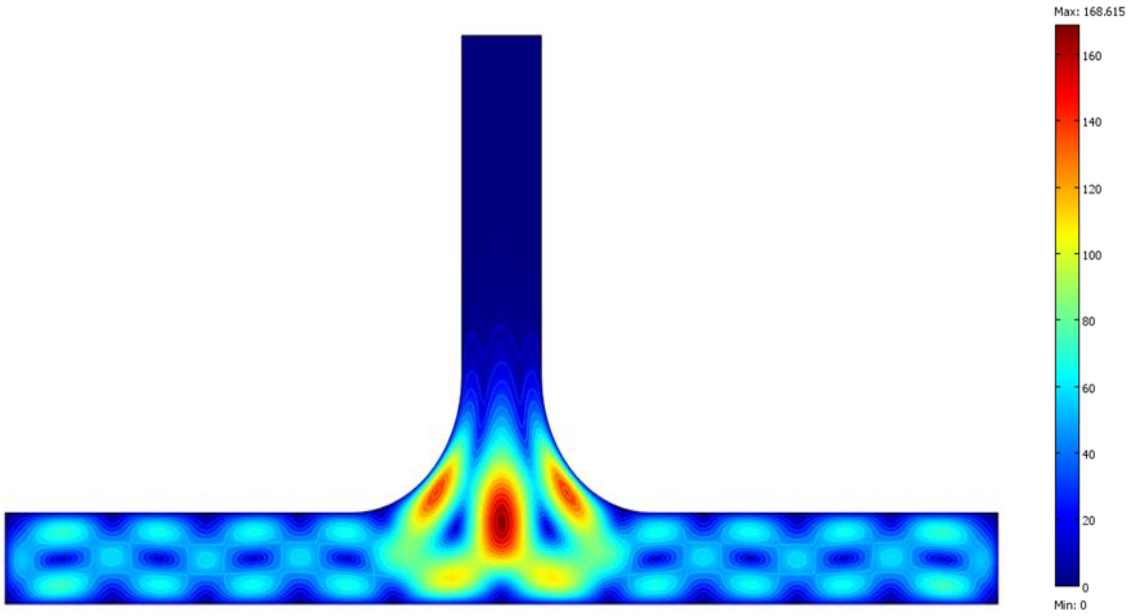

Figure 6: Dimensionless velocity field for Rc=0.24 and Ra=10^6

IV.2.2. Curved junction with major radius Rc = 0.34

figure (7) shows the isotherms for $Ra=10^4$ in this case temperature distribute as parallel lines indicating that the Pseudo-conduction heat transfer dominate the region, with more deformation intensity at the entry region of the chimney that demonstrates the presence of a weak natural convection, figure (8) represents velocity field distribution showing an approximately higher value compared to the first geometry for $Ra=10^4$, however the flow remain stagnant and no significant air motion throughout the chimney's tower.

Figure (9) illustrates isotherms for $Ra=5x10^5$ indicating an increase of natural convection in the entire system translated as a distortion of the isothermal lines throughout the system. Figure (10) shows more intensification of the counter rotating cells at the upper part of the chimney's entry mediated by a main cell moving upward representing a generation of the airflow under a convective mode.

Figures (11-12), represent a fully deformed isothermal lines and velocity field distributions that show a significant increase of the velocity of airflow generated which is manifested in close intense counter rotating cells located at the chimney's entry moving upward to the outlet all along the collector area considered as a zone of instabilities when the Rayleigh-Bénard phenomenon is observed. Noticing that this slight change in the junction's curvature radius and the significant increase of Rayleigh value contributed in the increase of the air motion smoothness thus the flow development compared to the previous geometry at the same Rayleigh value, confirming by which the full dominance of natural convection mode in the generation of the flow.

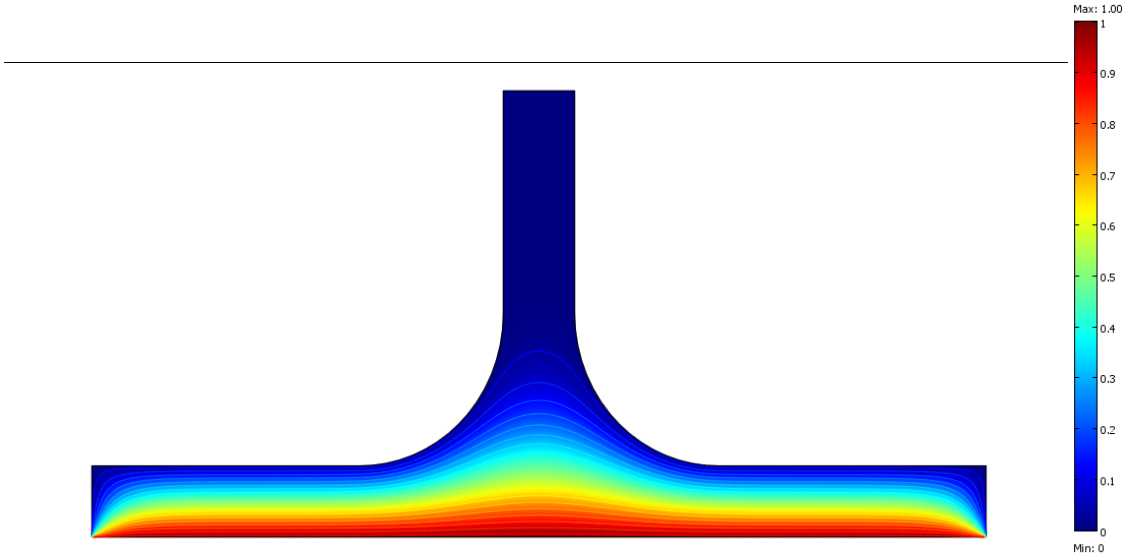

Figure 7: Dimensionless temperature distribution for Rc=0.34 and Ra=10^4

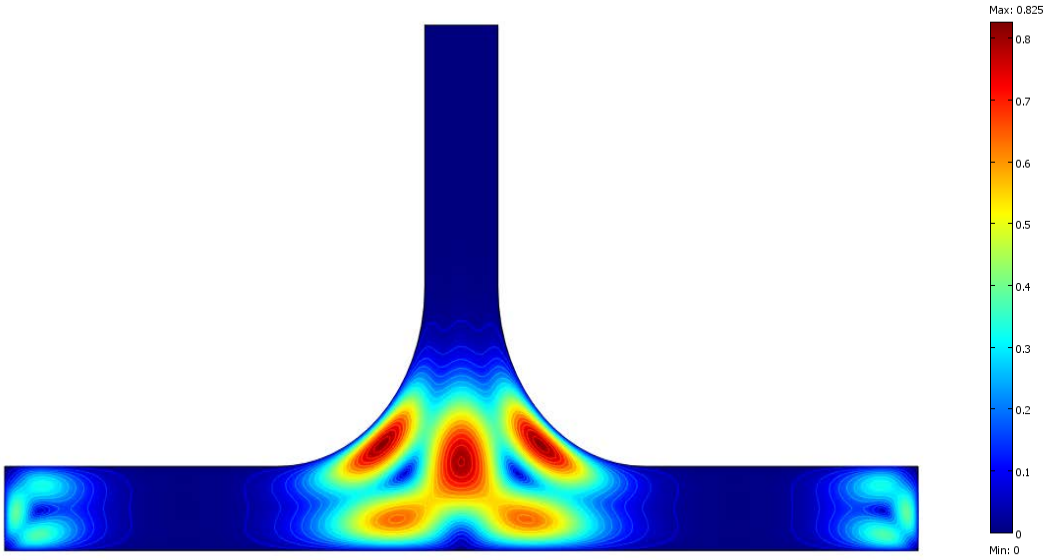

Figure 8: Dimensionless velocity field for Rc=0.34 and Ra=10^4

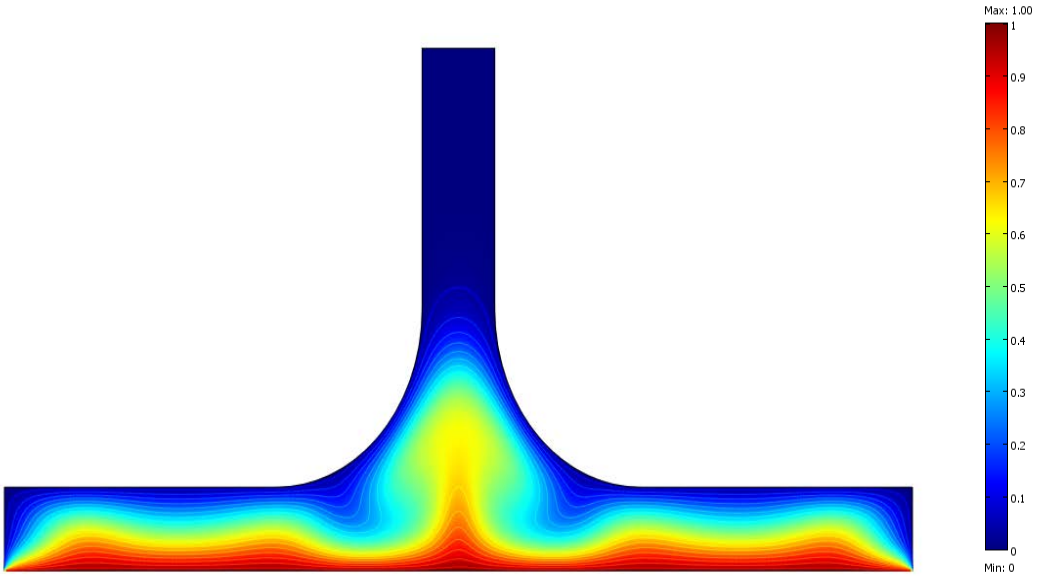

Figure 9: Dimensionless temperature distribution for Rc=0.34 and Ra=5x10^5

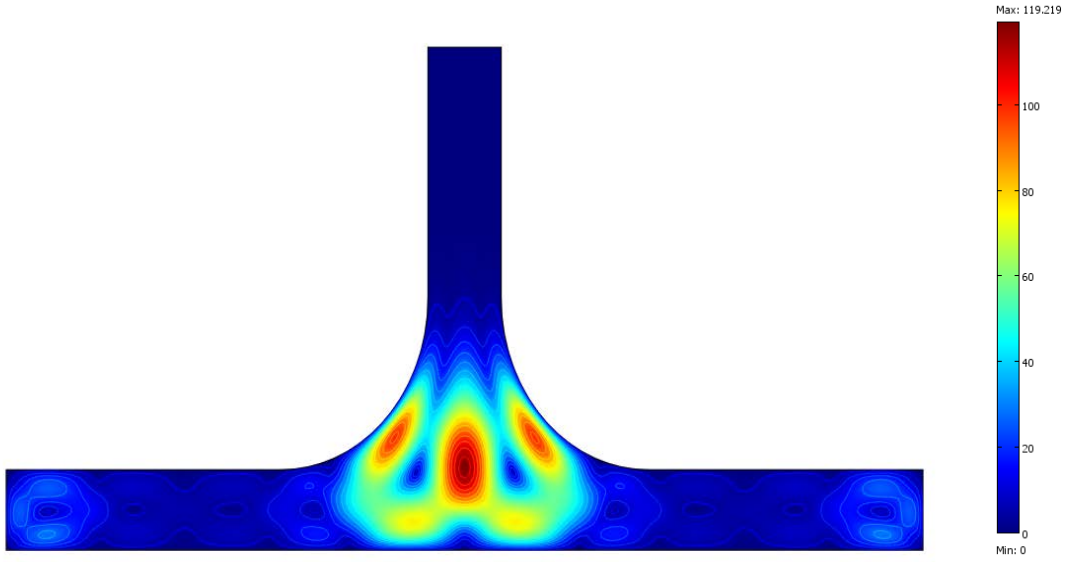

Figure 10: Dimensionless velocity field for Rc=0.34 and Ra=5x10^5

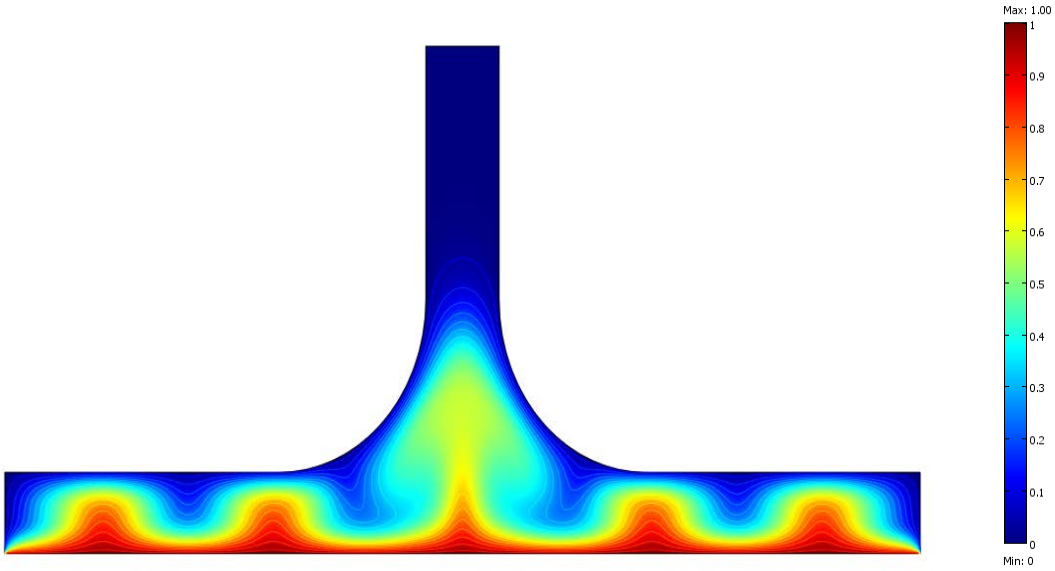

Figure 11: Dimensionless temperature distribution for Rc=0.34 and Ra=10^6

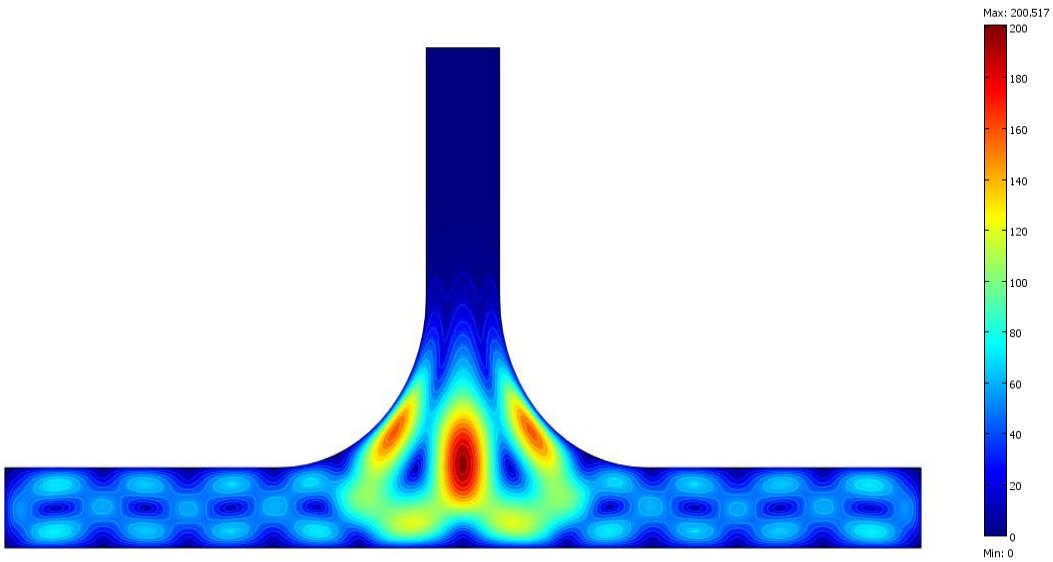

Figure 12: Dimensionless velocity field for Rc=0.34 and Ra=10^6

IV.2.3. Curved junction with major radius Rc = 0.44

Figure (13) shows the isotherms for $Ra=10^4$ in this case isotherms are parallel lines indicating the pseudo-conduction mode in this region, noticing a slight deformation in the entry region of the chimney that demonstrates the presence of a natural convection and a remarkable relative increase in airflow velocity at the entry region of the chimney and at the inlets region compared the previous geometries represented in figure (14).

When Rayleigh values increased to $Ra=5x10^5$ and $Ra=10^6$. We have a significant intensification of the natural convection mode in the entire space manifested in the full distortion of isotherms in figures (15) and (17) announcing a presence of significant airflow field illustrated in figure (16) and (18), as close intense counter rotating cells located at the chimney's entry moving smoothly upward to the outlet indicating the presence of Rayleigh-Bénard phenomenon.

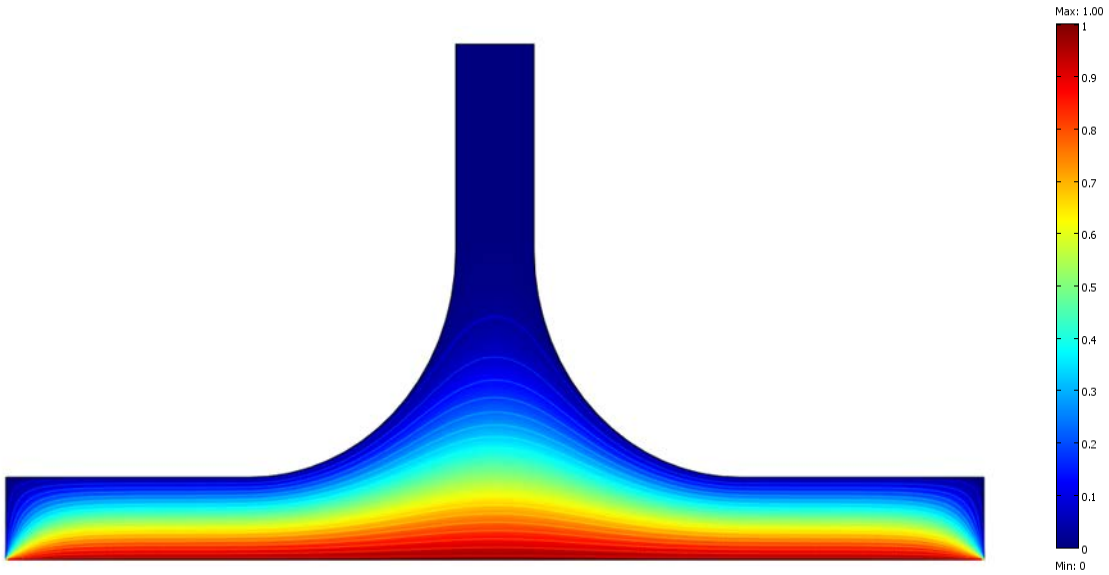

Figure 13: Dimensionless temperature distribution for Rc=0.44 and $Ra=10^4$

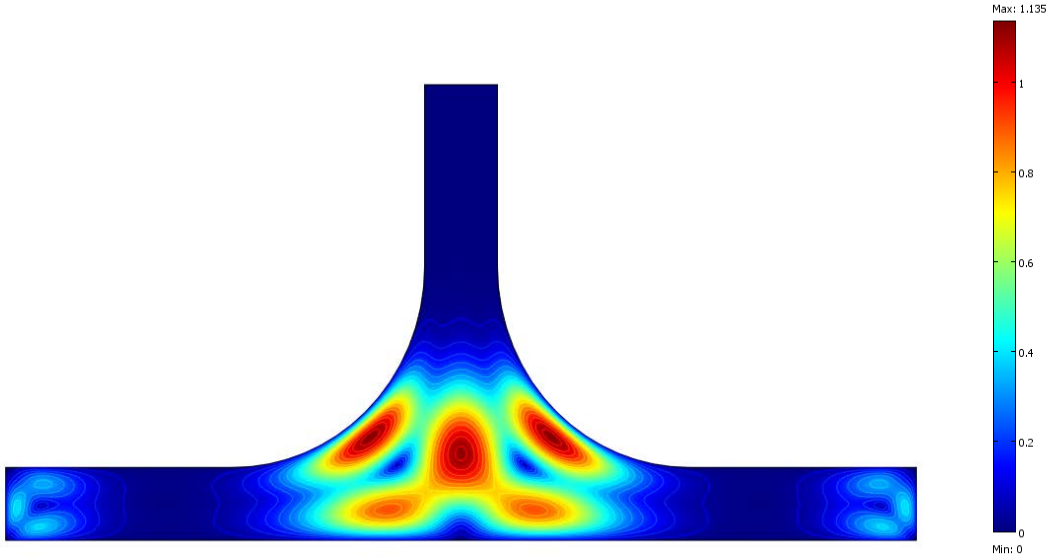

Figure 14: Dimensionless velocity field for Rc=0.44 and Ra=10^4

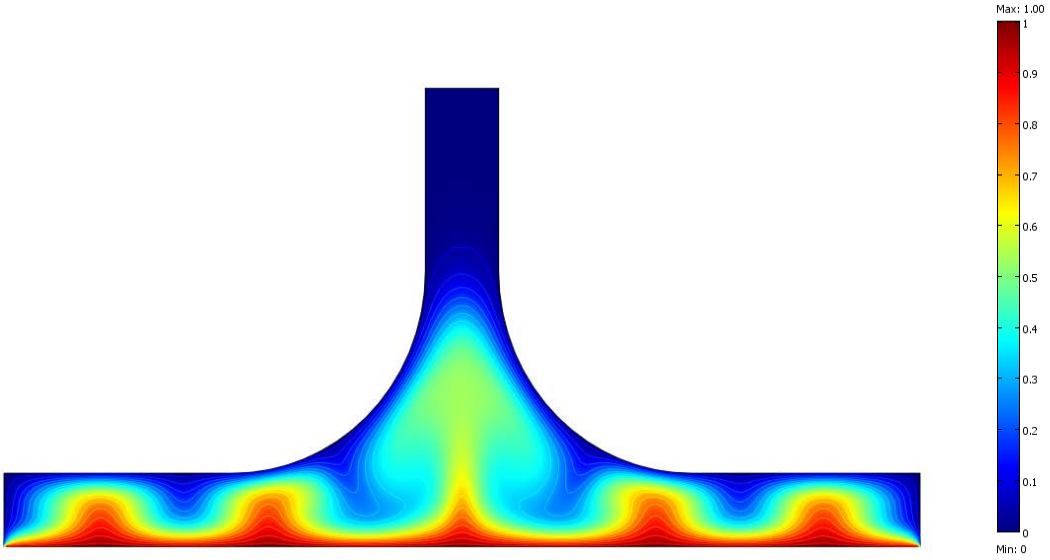

Figure 15: Dimensionless temperature distribution for Rc =0.44 and Ra=5x10^5

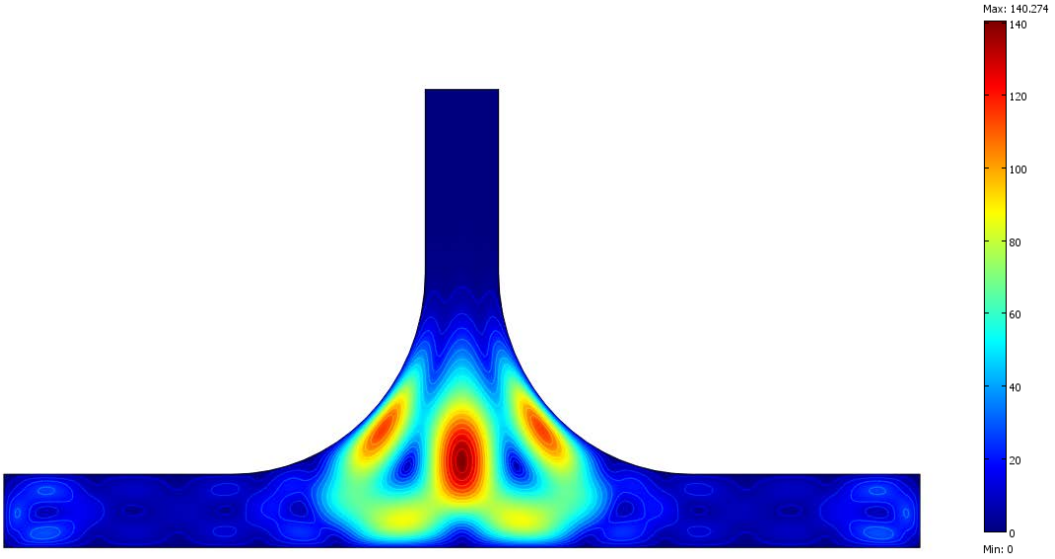

Figure 16: Dimensionless velocity field for Rc=0.44 and Ra=5x10^5

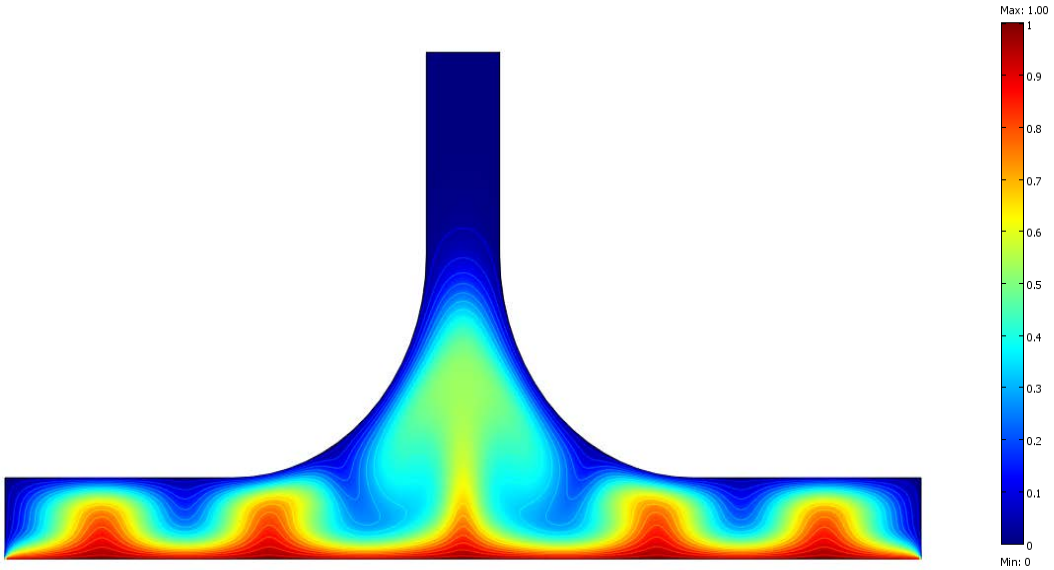

Figure 17: Dimensionless temperature field for Rc=0.44 and Ra=10^6

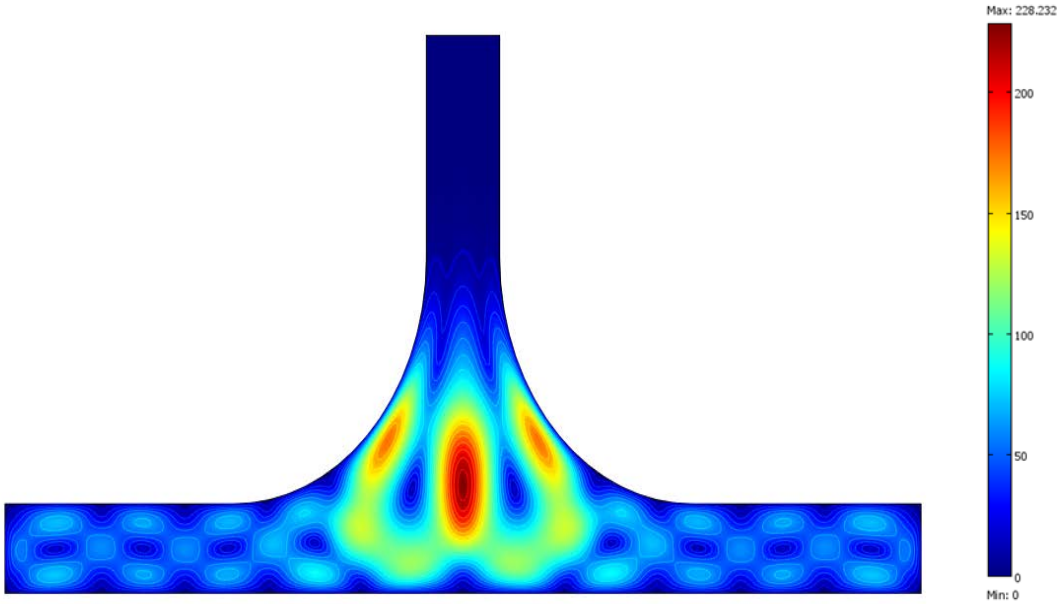

Figure 18: Dimensionless velocity field for Rc=0.44 and Ra=10^6

IV.2.4. Curved junction with major radius Rc = 0.54

At Ra=10^4 isotherms in figure (19) are paralleled lines indicating the mode of pseudo-conduction in the collector area, while we note slight deformation in the entry region of the chimney that demonstrates the presence of a noticeably greater natural convection compared to the previous geometries for Ra=10^4 illustrated in figure (20) as counter rotating cells representing by which air flow velocity field distribution, that flow is still stagnant and not generated due to the insignificant air motion in the space.

Figures (21) and (23) illustrate isotherms for Ra=5x10^5 and Ra=6x10^5 respectively as a significantly increase in the distortion of the isothermal lines throughout the system with more intensively at the chimney's entry region This indicates dominance of natural convection mode in the entire space due to due to the larger free space. Figures (22) and (24) shows intensification of the counter rotating cells in the chimney's entry and moving upward to the outlet and spins in the collector area representing an appreciable and relatively regular increase in the airflow field intensification. In particular for this case of a larger curvature radius with Rc=0.54, the computation has shown a limitation in the Rayleigh number increase which reached a limit of Ra= 6x105 instead of Ra=106 for the previous case of curvature radius. This behavior is mainly due to the evolution of the natural convection from a laminar

to a turbulent flow above this value of Rayleigh number while the model selected in Comsol is laminar and the computation has not converged above this value.

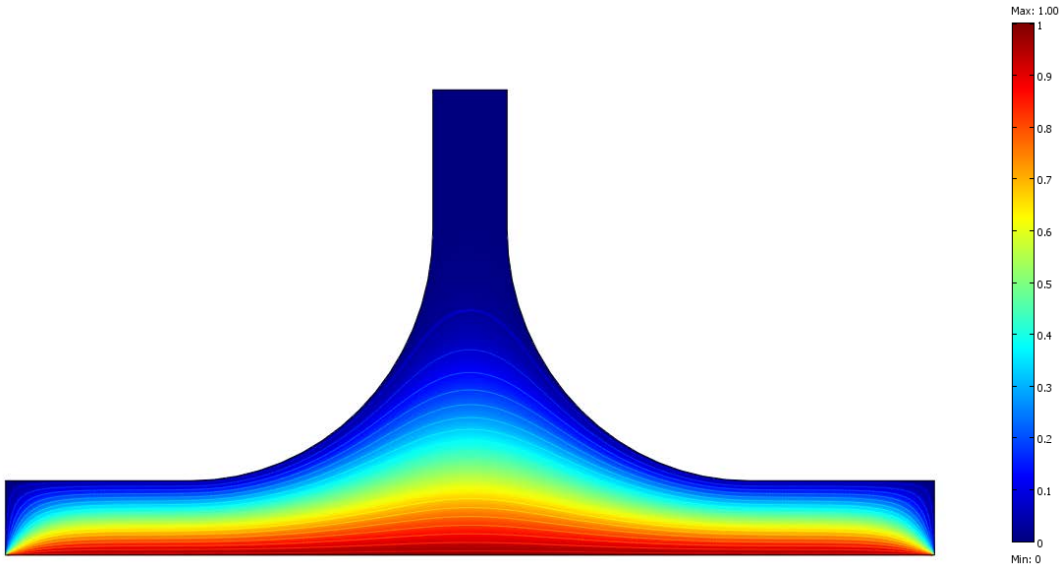

Figure 19: Dimensionless temperature distribution for Rc=0.54 and Ra=10^4

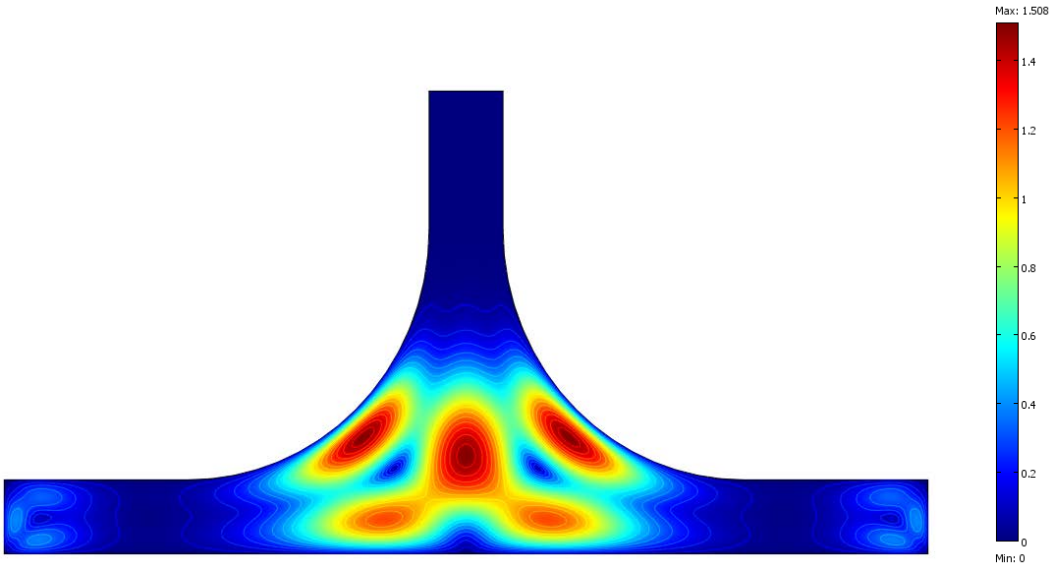

Figure 20: Dimensionless velocity filed for Rc=0.54 and Ra=10^4

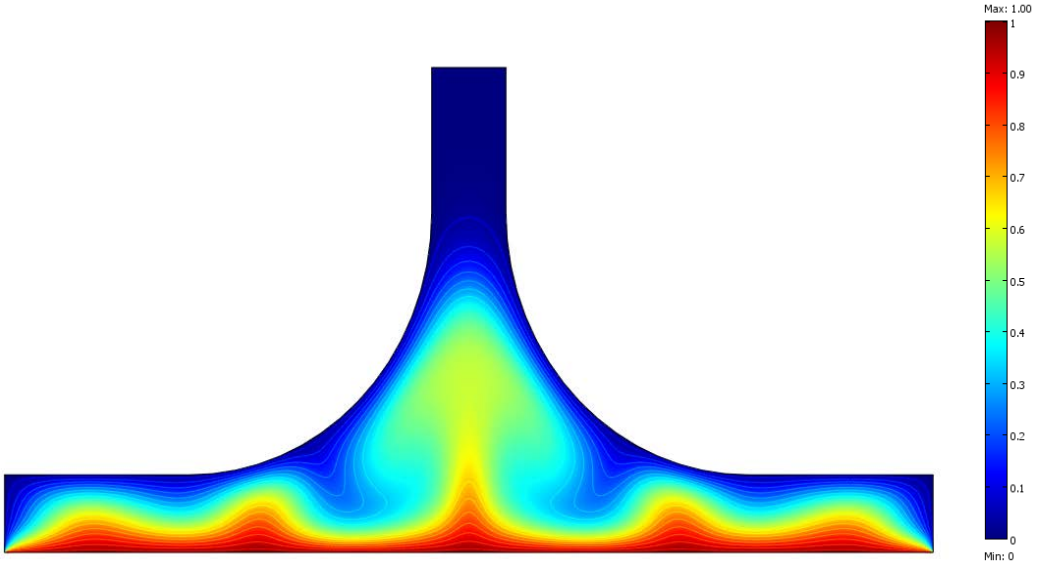

Figure 21: Dimensionless temperature distribution for Rc=0.54 and Ra=5x10^5

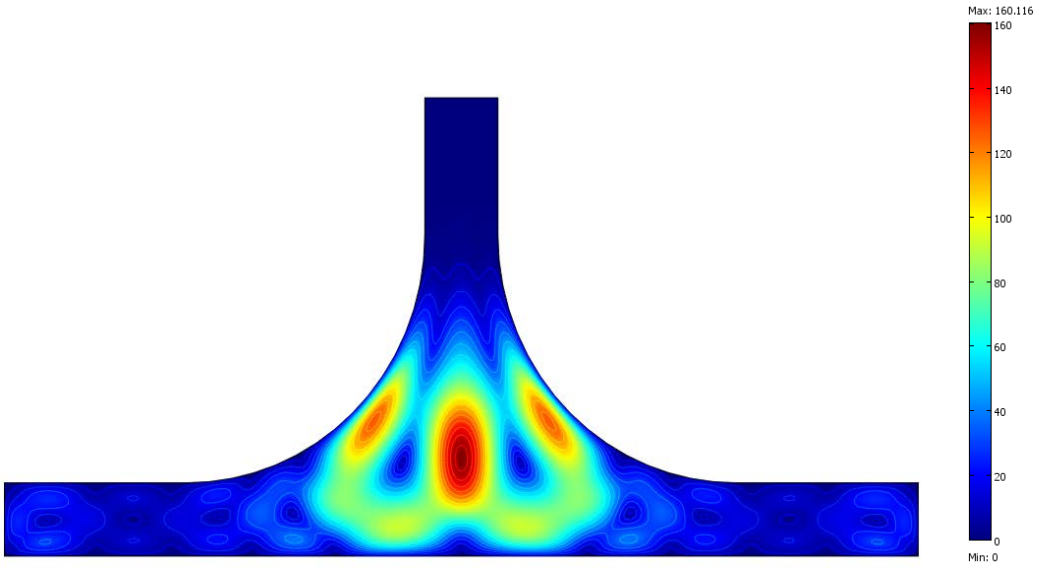

Figure 22: Dimensionless velocity field for Rc=0.54 and Ra=5x10^5

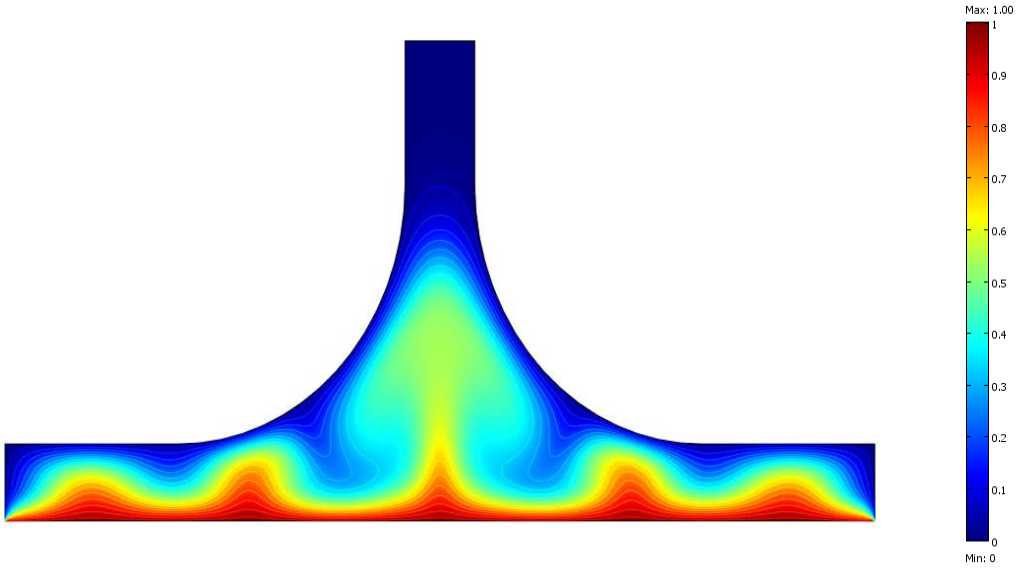

Figure 23: Dimensionless temperature distribution for Rc=0.54 and Ra=6x10^5

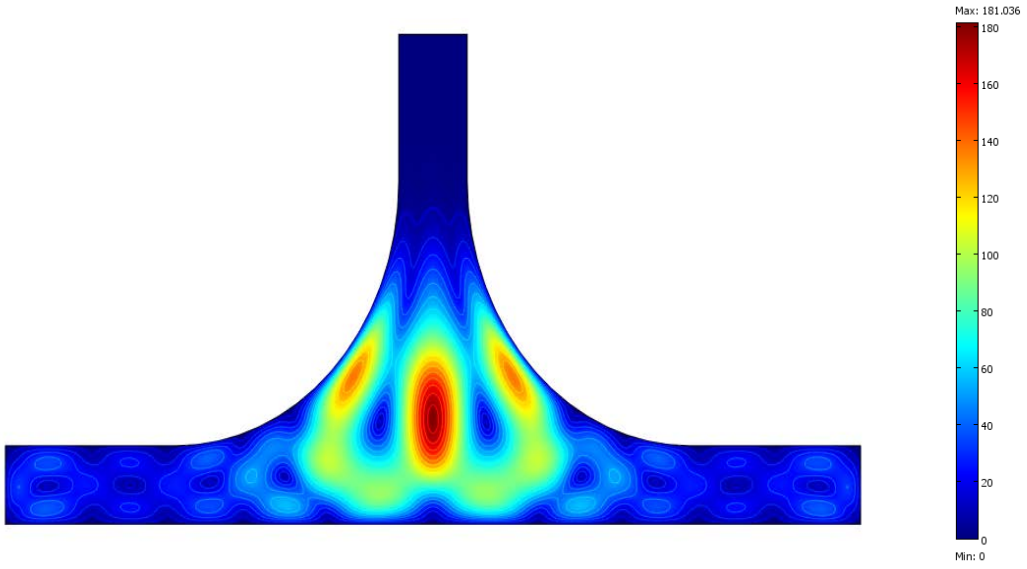

Figure 24: Dimensionless velocity field for Rc=0.54 and Ra=6x10^5

IV.2.5. Fully curved chimney surface with hyperbolic profile

Figure (25) describes isotherms for Rayleigh value of $Ra=10^4$ for the case of fully curved shape of the solar chimney, figure shows that isothermal lines are still following the walls profiles and the temperature decreases from the hot section (the ground) to the cold one (the roof) indicating by which that the heat transfer is dominated mainly by the pseudo-conduction mode, except for the chimney's entry region we notice a slight distortion announcing a presence of air motion therefore a low intense natural convection manifested either in figure (26) as counter rotating cells located in the chimney's entry and a noticeably very low intense cells at the inlet regions of the collector with an approximately lower value compared to the previous curvature cases.

Figure (27) shows that isothermal lines are no more parallel and deformed intensively all along the collector area and significantly at the chimney's entry indicating that natural convection contributed effectively all along the system.

Figure (28) represents the velocity field distribution for $Ra=5x10^5$ with more intensity counter rotating cells compared to the one with $Ra=10^4$ and decreased significantly to be equivalent approximately to the geometry with Rc= 0.44, indicating a presence of significantly increased airflow but weaker than the previous one which is confirmed in the distribution profile of velocity of $Ra=7x10^5$ in figures (29-30), where a full distortion of the isothermal lines demonstrating the dominance of the natural convection heat transfer, and an appreciable airflow at the chimney's entry and more swirls in the collector area. Noticing that at Rc = 0.54, the system's air flow reached its maximum limitation (peak) and started to progressively reduce. Thus, the air flow development within the solar chimney depends on the Rayleigh's value and the control of junction's curvature radius.

Following the same behavior noticed in the previous case where the Rayleigh number has reached a peak of $Ra= 6x10^5$, in this case of hyperbolic shape of the solar chimney walls the Rayleigh number has reached a limit of $Ra= 7x10^5$ instead of $Ra=10^6$. This is mainly due to the evolution of the natural convection from a laminar to a turbulent flow above this value similarly to the previous case, the Comsol model has not converged above these values.

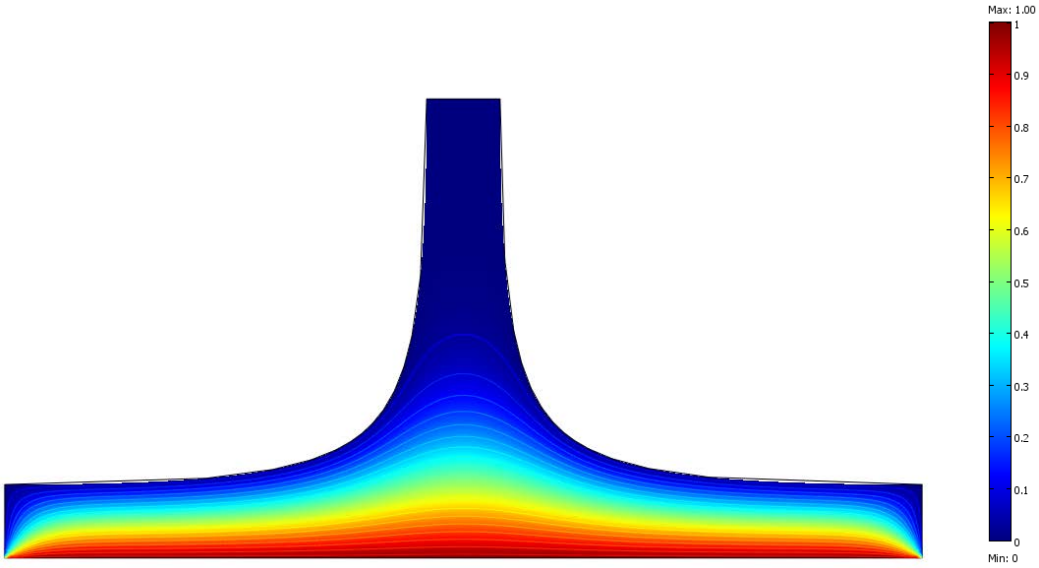

Figure 25: Dimensionless temperature distribution with Ra=10^4 for the fully curved chimney

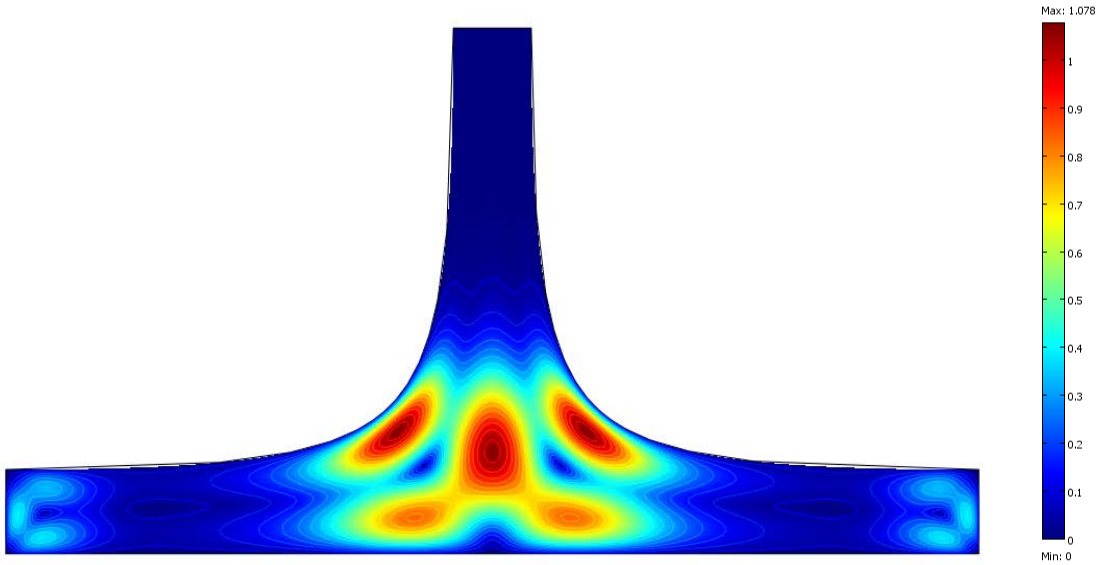

Figure 26: Dimensionless temperature distribution with Ra=10^4 for the fully curved chimney

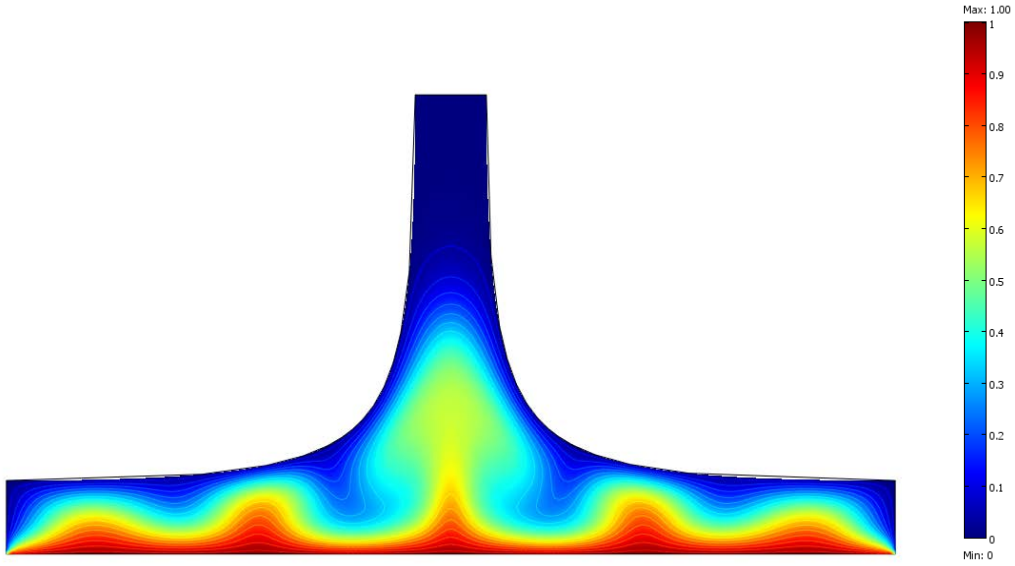

Figure 27: Dimensionless temperature distribution with Ra=5x10^5 for the fully curved chimney

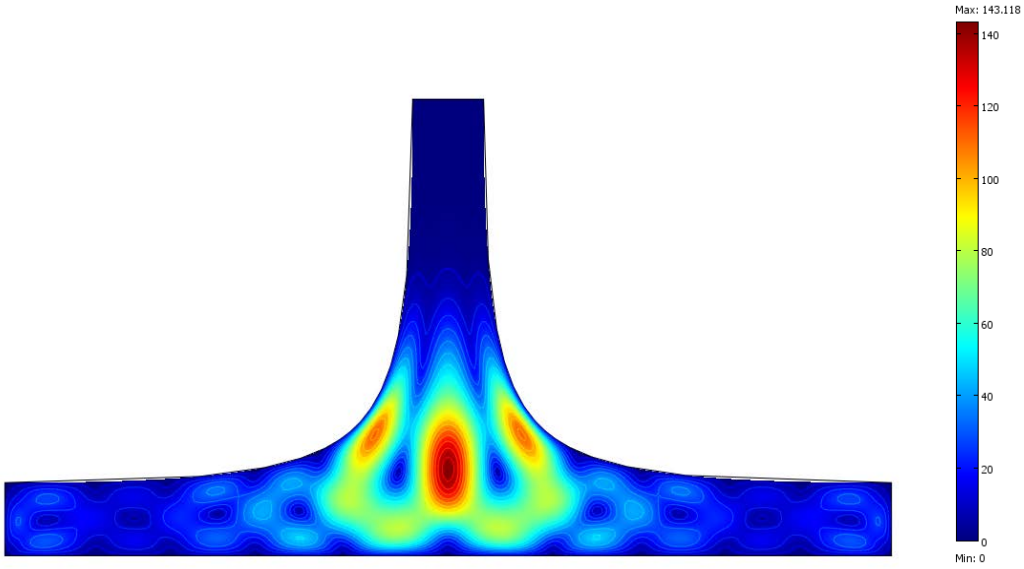

Figure 28: Dimensionless velocity filed with Ra=5x10^5 for the fully curved chimney

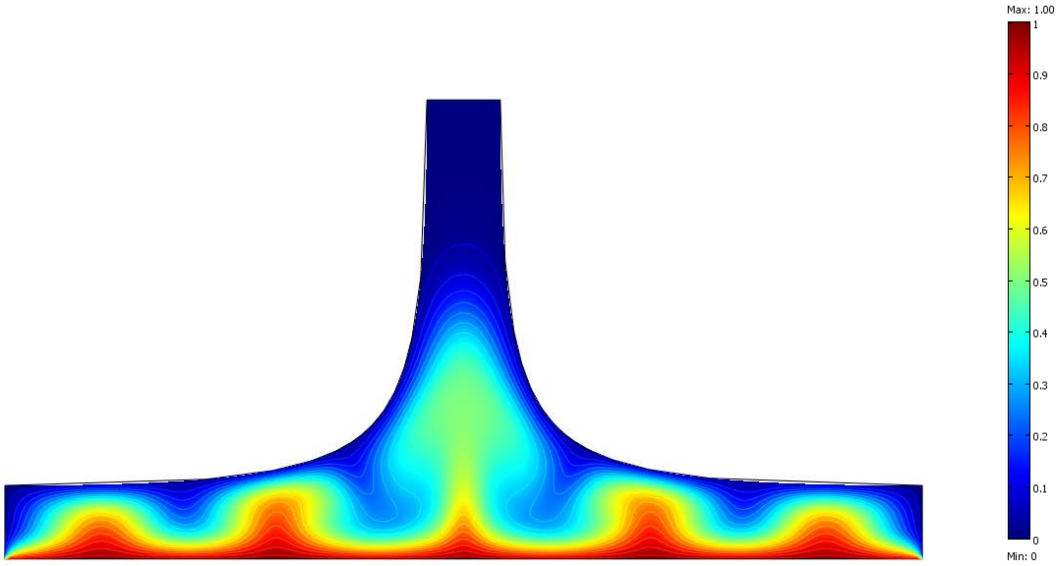

Figure 29: Dimensionless temperature distribution with Ra=7x10^5 for the fully curved chimney

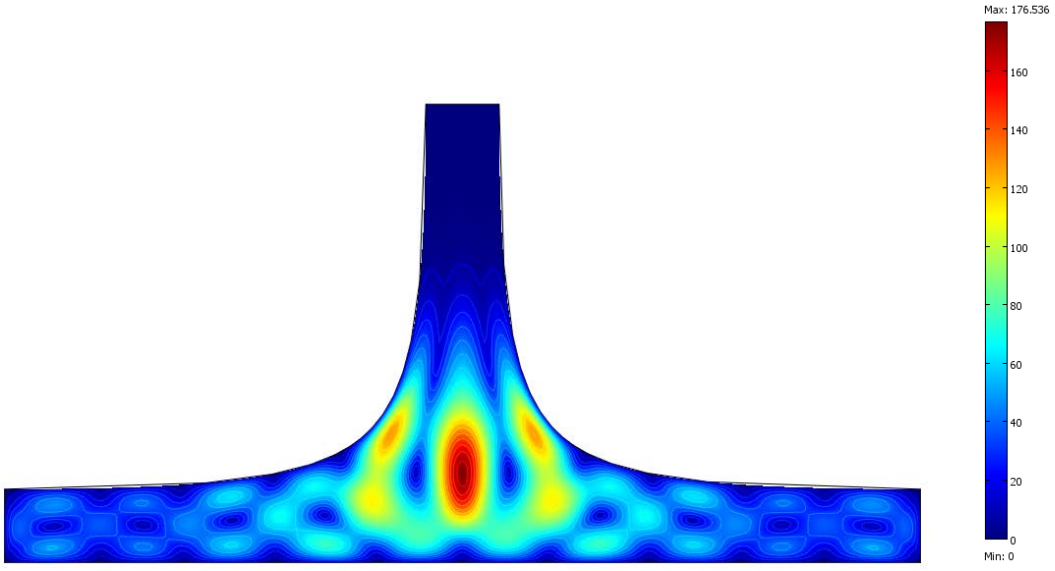

Figure 30: Dimentionless velocity field with Ra=7x10^5 for the fully curved chimney

IV.3. Effect of Rayleigh number on airflow vertical velocity

Figures (31-35), show profiles of the air dimensionless vertical velocity for different Rayleigh values at a fixed junction curvature radius, whereby we note that the velocity vary increasingly according to the Rayleigh number value and the control of the junction's curvature radius until it reaches a specific maximum value in the chimney's tower.

Taking for example, the first geometry case with Rc = 0.24 illustrated in figure (31), we note an appreciable evolution in vertical velocity magnitude reaching a value of V^{+}=10 when Ra= 10^5 and V^{+}=170 when Ra=10^6, this maximum velocity reaches a highest point in the tower that correspond to Z^{+}=0.21 then start dropping dramatically towards the outlet.

Following the same analyses approach with further increase of the curvature radius to Rc = 0.44 the maximum vertical velocity increases significatively by more than 500% when Ra is increased from 10^5 to 10^6 this increase is mainly due to the intensification of the flow under the fully developed convective mode which leads us to conclude that the airflow motion throughout the chimney is directly correlated and positively proportional to the Rayleigh number that characterize the intensity of the natural convection.

From figures (31-35), we can also notice that below a certain value of Rayleigh number and regardless the curvature radius, the heat transfer is mainly conducted by pseudo conductive mode and the air within the entire space of the chimney is stagnant. This value correspond in our case study to Ra=10^5 which represent a critical value representing a transition border from pseudo conductive to fully convective mode.

The location of the maximum vertical velocity within the chimney defines the position of the turbine in order to collect the maximum kinetic energy for the airflow. In our case this position in the tower correspond to Z^{+} = +/- 0.2 regardless the intensity of the convection characterized by the value of Ra and regardless the chimney geometry that is characterized by the curvature radius of the junction Rc.

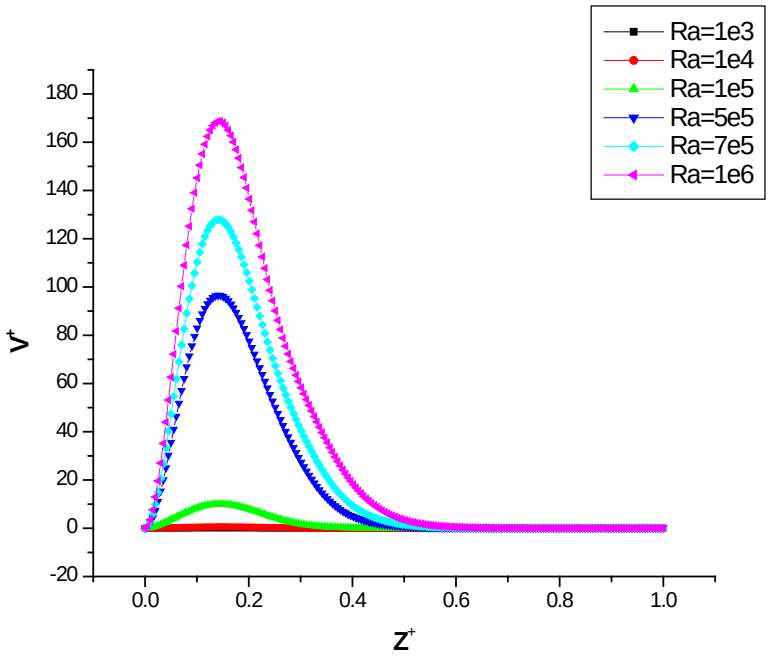

Figure 31: Dimensionless vertical velocity (V^+) for different Ra with curvature radius Rc=0.24

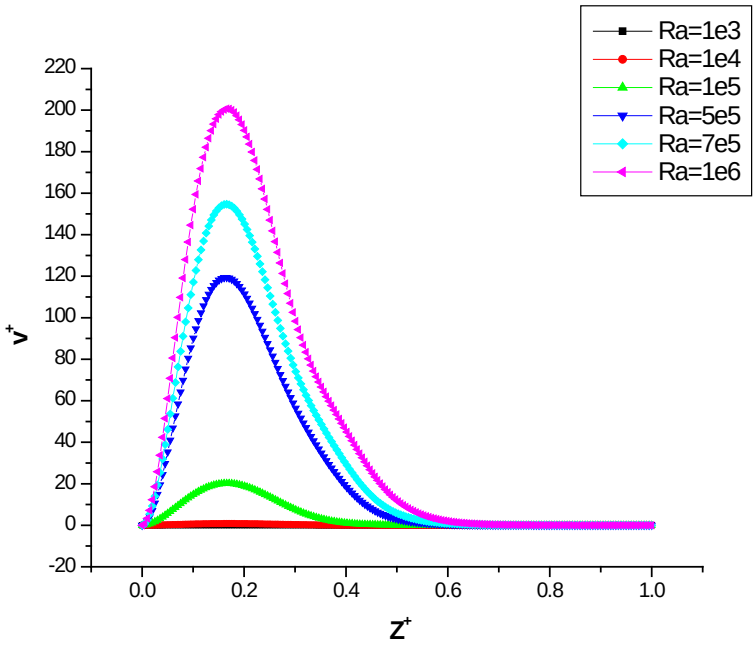

Figure 32: Dimensionless vertical velocity (V^+) for Ra with curvature radius Rc=0.34

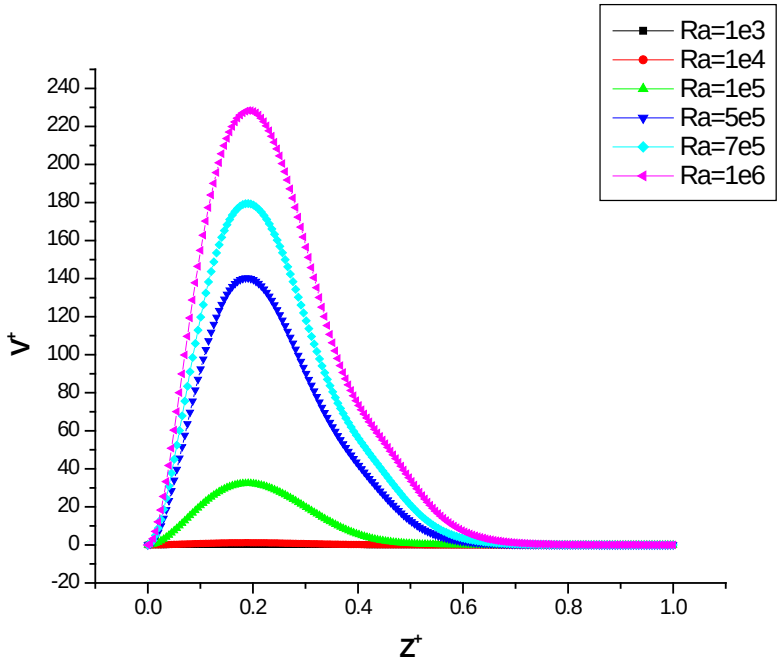

Figure 33: Dimensionless vertical velocity (V^+) for different Ra with curvature radius Rc=0.44

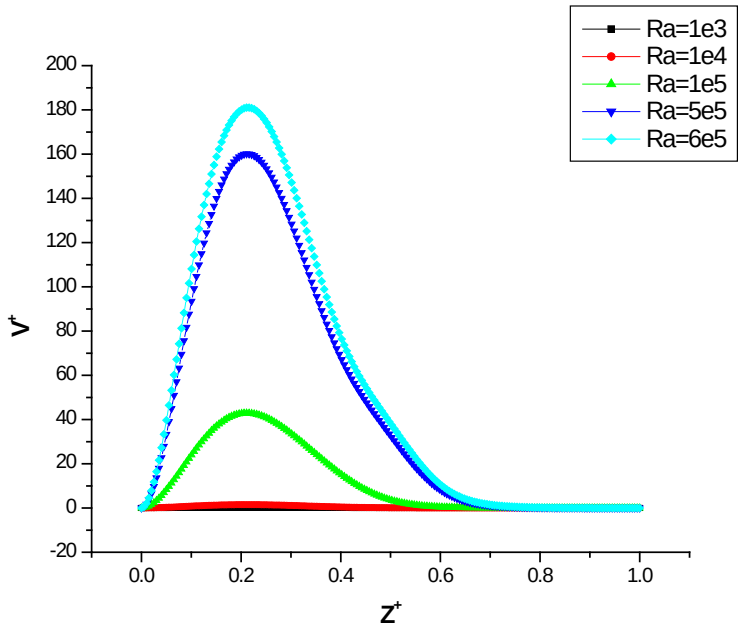

Figure 34: Dimensionless vertical velocity (V^+) for different Ra with curvature radius Rc=0.54

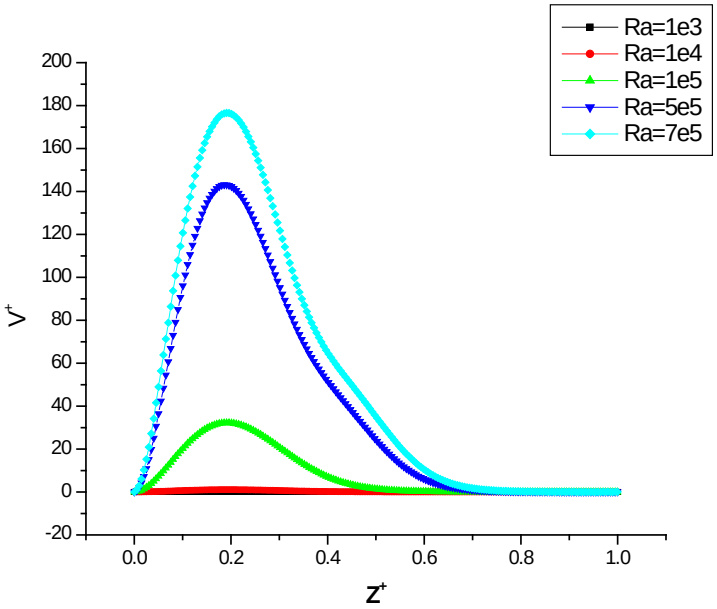

Figure 35: Dimensionless vertical velocity (V^+) for different Ra and for the case of fully curved chimney

IV.4. Effect of the junction curvature radius on airflow vertical velocity

We note that the variation of the curvature radius affect the airflow development throughout the free space within the solar chimney. The finest example of this is illustrated in figure (36) where we presented the dimensionless velocity magnitude V^+ in terms of the dimensionless vertical coordinate Z^+. Obviously we can notice that the velocity increases propositionally with the increase of the junction curvature radius Rc. It's also noticeable that both cases of fully curved solar chimney and curvature radius of Rc = 0.44 are almost matching. According to the first case for Rc=0.24 the maximum velocity reaches dimensionless value of 96 at position of Z^+=0.14 that correspond to height in the chimney tower. In the second case for Rc = 0.34 the dimensionless velocity reach a maximum value of 119 at Z^+=0.16 following the same evolution and for Rc=0.54 the velocity reaching its maximum slightly above 160 at Z^+=0.21, the curvature radius increase from Rc=0.24 to Rc=0.54 has positively affected the solar chimney performance by increasing the vertical velocity with an estimated rate of 67%. This behavior help us to conclude that the solar chimney performance is strongly correlated to the junction radius variation and the potential loss of kinetic energy depends on the free space created by the shape of the junction that let the airflow rise smoothly throughout the tower. Thus the best and efficient performance is achieved in our case correspond the maximum curvature radius Rc = 0.54.

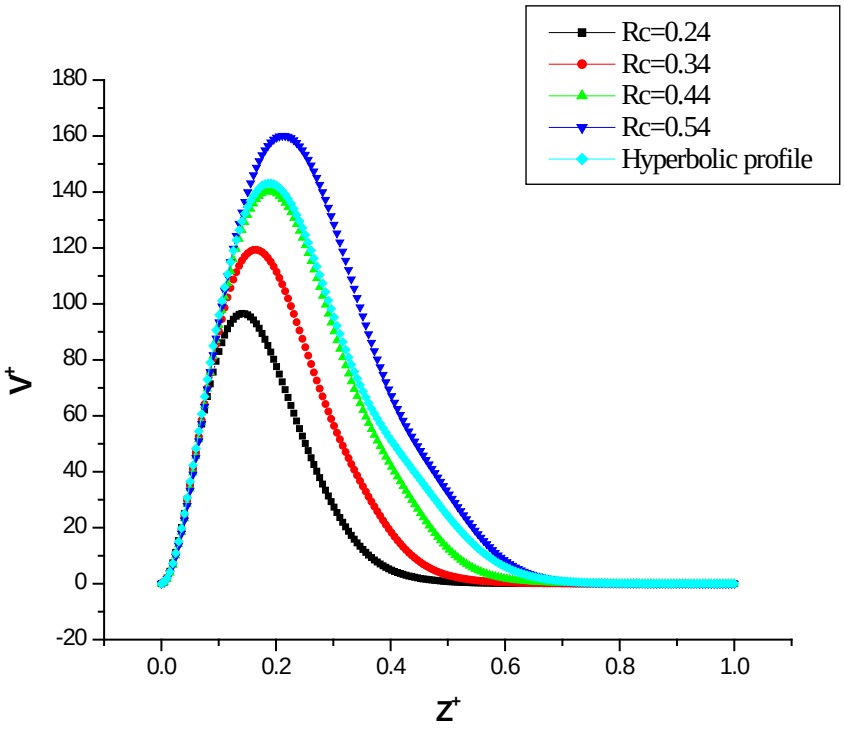

Figure 36: Dimensionless vertical velocity ($V^{+)}$ for different curvature radius Rc with Ra=5x10^5

IV.5. Effect of the collector height H on temperature and velocity isolines

Figures (37-46) represent the dimensionless temperature and velocity distributions for Rayleigh value Ra=5x10^5 and for different heights H in a range of [0.05-0.25]. For the case of H=0.05 isotherms are parallel lines in the space between the collector and the ground, the heat transfer is mainly generated by pseudo conduction with slight distortion at the chimney's entry indicating the presence of a very weak natural convection. The isotherms distortion in the chimney's entry indicating a development of naturel convection at this instability zone while heat transfer remain conductive at the collector area due to the limited free space that slowdown the airflow development which have a significant rate at the chimney's entry. With increasing in the collector height to H=0.1 and H= 0.15 both temperature and velocity fields has not represent a significant changes within the collector space while an intensification of the natural convection occurred at the chimney's entry. With a further increase in the collector height to H=0.2 and H=0.25, the natural convection become fully developed in the entire space of the solar chimney. As clearly shown in figures 43-46 the temperature and the velocity fields are resulting from a fully developed flow under a

convective mode with an intensification of cells at the chimney's entry and at the inlet regions under the collector roof.

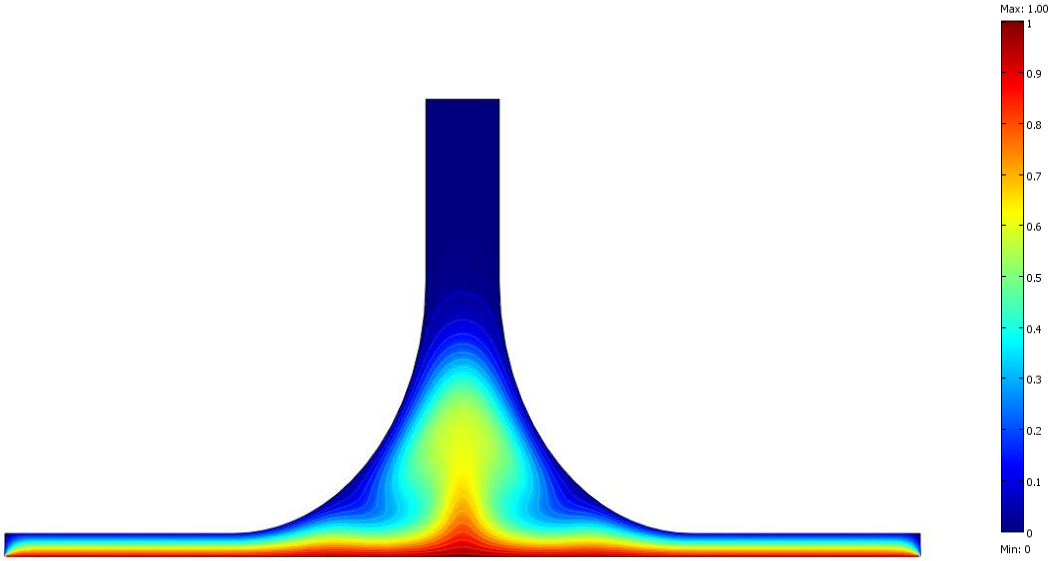

Figure 37: Dimensionless temperature distribution with H=0.05 and Ra=5x10^5

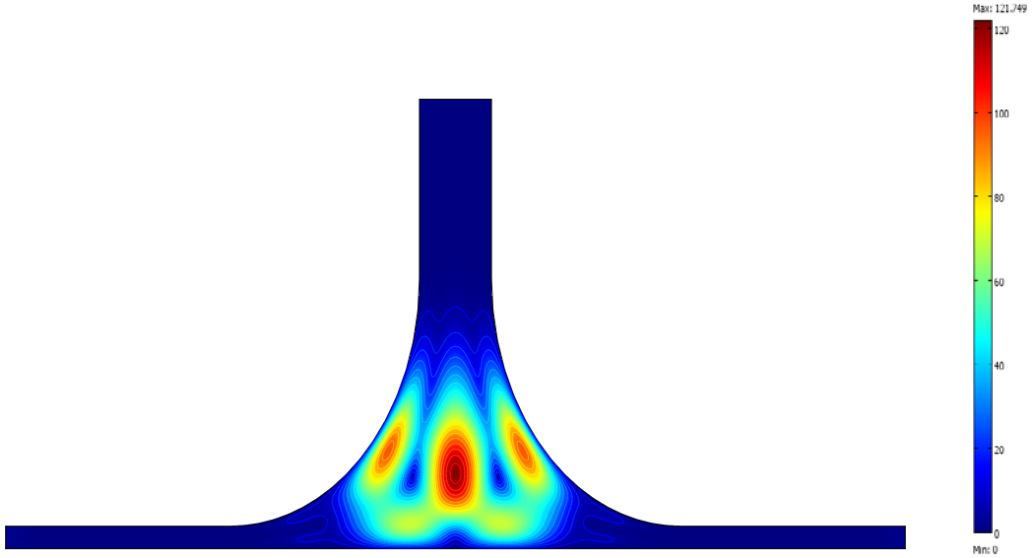

Figure 38: Dimensionless velocity field with H= 0.05 and Ra=5x10^5

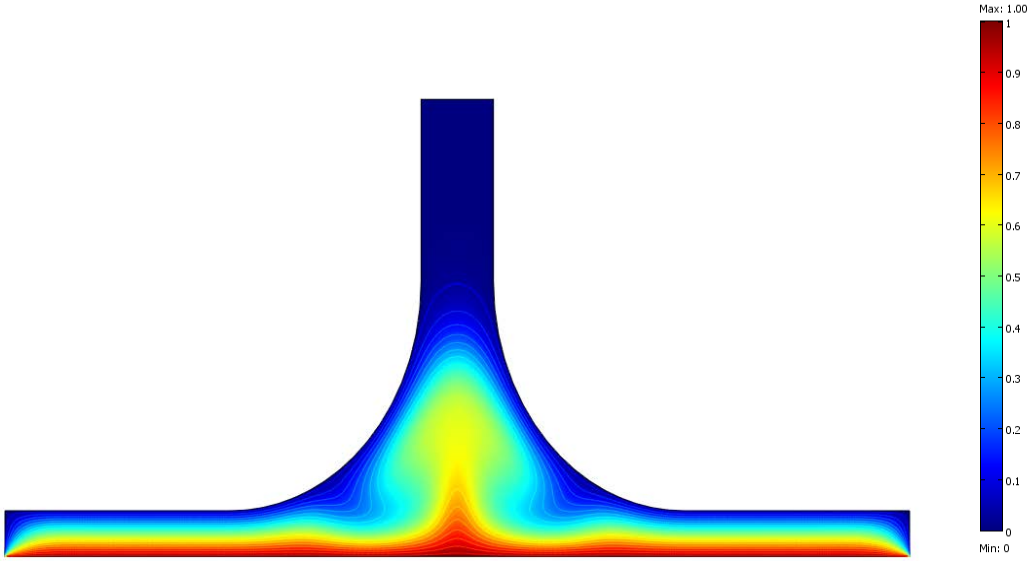

Figure 39: Dimensionless temperature distribution with H=0.1 and Ra=5x10^5

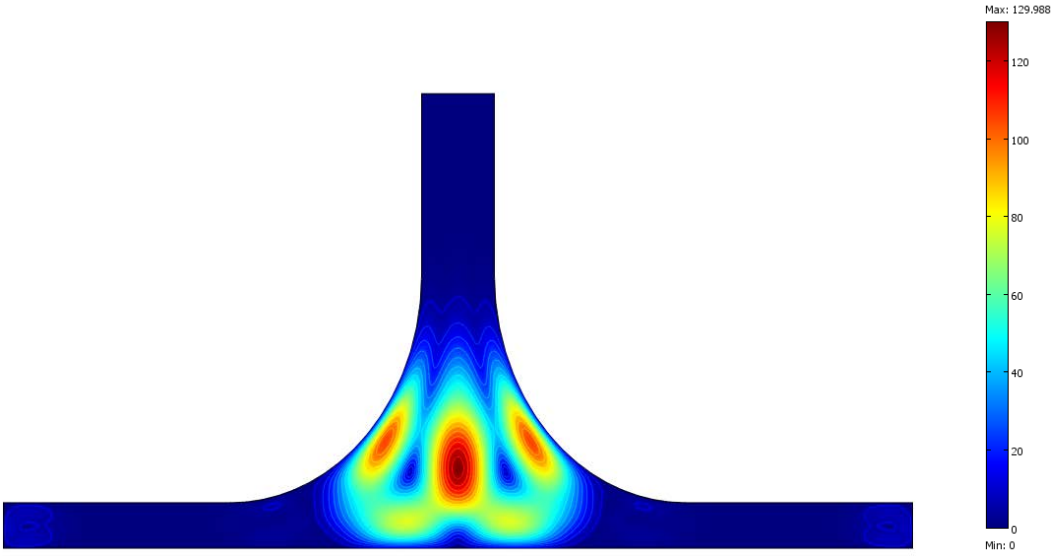

Figure 40: Dimensionless velocity distribution with H= 0.1 and Ra=5x10^5

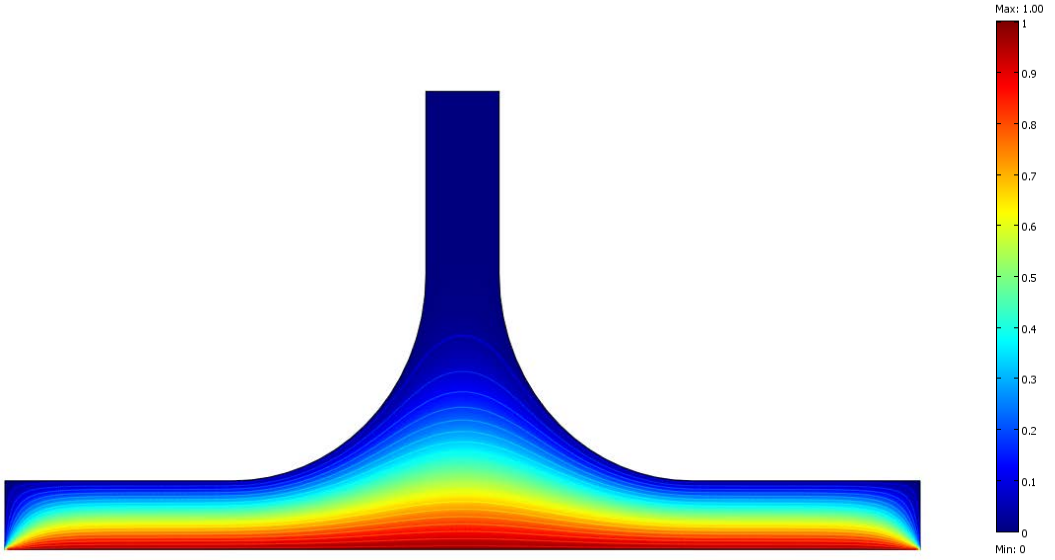

Figure 41: Dimensionless velocity distribution for H=0.15 and Ra= $5x10^5$

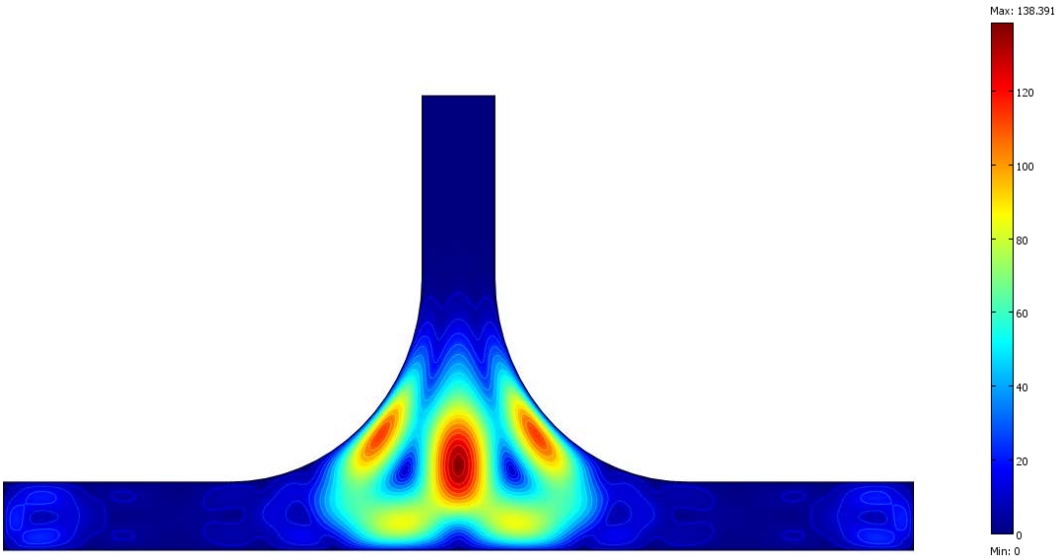

Figure 42: Dimensionless velocity field for H=0.15 and Ra= $5x10^5$

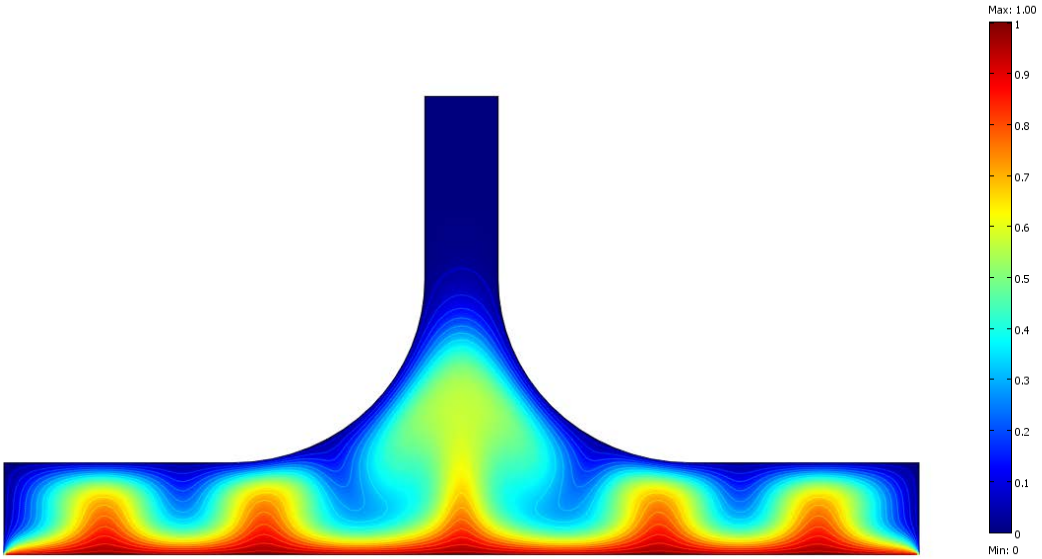

Figure 43: Dimensionless temperature velocity for H=0.2 and Ra=5x10^5

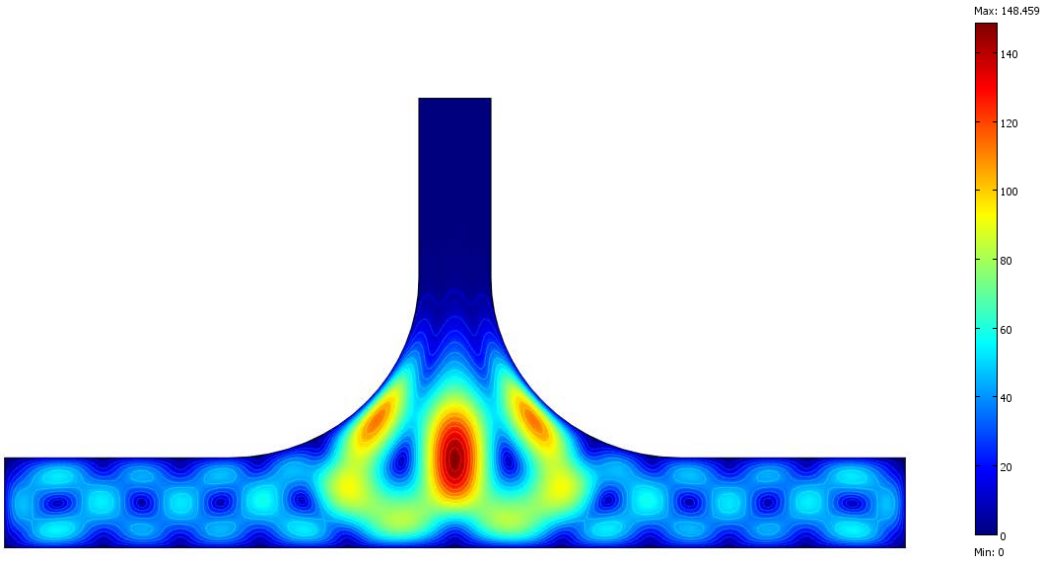

Figure 44: Dimensionless velocity field for H=0.2 and Ra=5x10^5

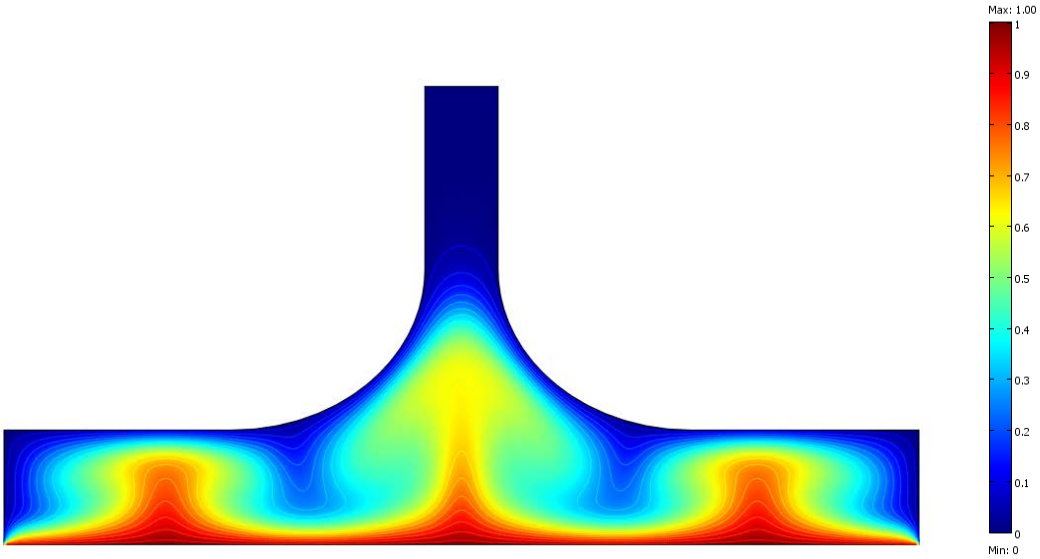

Figure 45: Dimensionless velocity field for H=0.25 and Ra=5x10^5

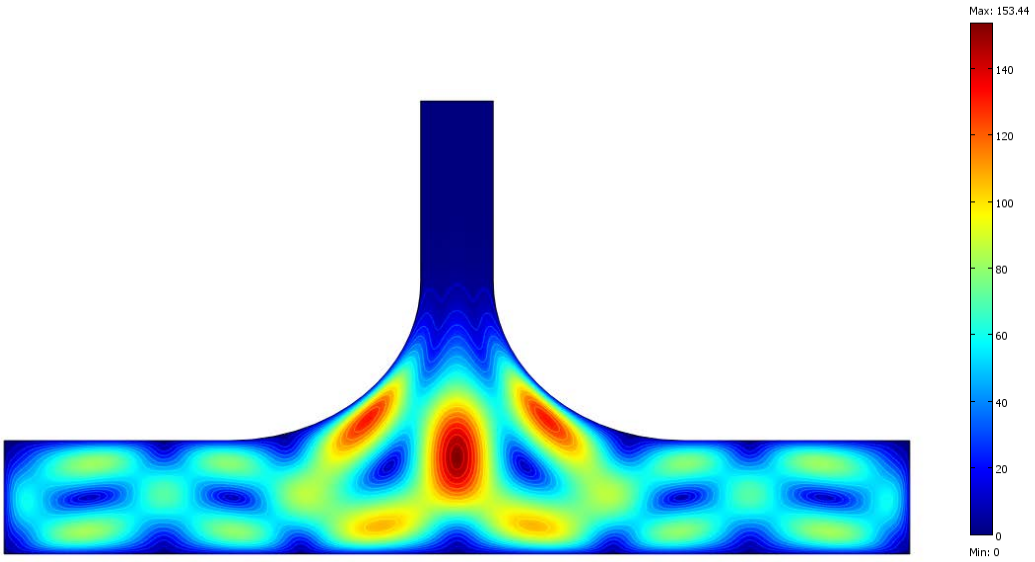

Figure 46: Dimensionless velocity field for H=0.25 and Ra=5x10^5

IV.6 Effect of the collector height H on airflow vertical velocity

Through the figure 47, which represent dimensionless vertical velocity of the airflow profiles for different height values at fixed Rayleigh value of $Ra=5x10^5$. We see that raising the height of the collector allows for the airflow to develop freely throughout the space, velocity magnitude vary increasingly until reaching a curtain altitude in the chimney than the airflow intensity start dropping gradually till reaching a motionless state near the outlet, according to the first case for H=0.05, the velocity peak reaches 121 compared to the velocity value of 153 for height of H =0.2 this height increase gives an improvement in the airflow vertical velocity close to 27%. The solar chimney performance is positively correlated to the collector's height geometry, the solar chimney's efficiency improved as the collector's height increased.

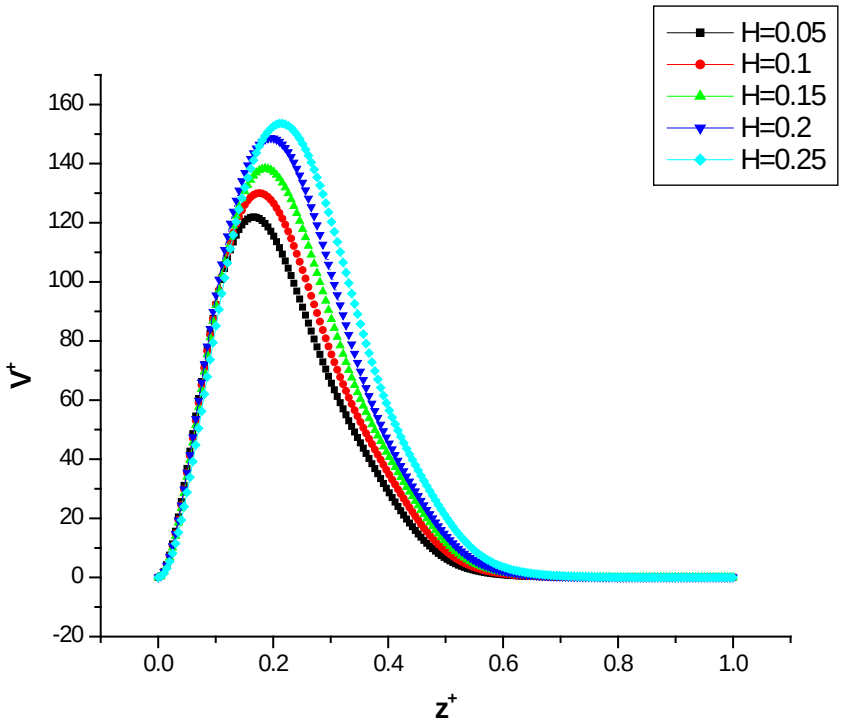

Figure 47: Dimensionless vertical velocity (V^+) for different collector height values with $Ra=5x10^5$

CONCLUSION

We provided a numerical simulation of a bi-dimensional axisymmetric solar chimney using Comsol Multiphysics Software in the current parametric research, in order to compute the air flow generated by natural convection within the solar chimney applying the boussinesq approximation and the relevant assumptions including the laminar flow of the fluid that is regarded permanent, Newtonian and incompressible as well as mathematical formalisms using PDE system in cylindrical coordinates.

The current work focuses on the influence of Rayleigh variation on the natural convection within the solar chimney as well as the geometrical parametric effects of the solar chimney on the system's efficiency which depend essentially on the airflow vertical velocity; the geometrical parameters in our case are the height of the collector as well as the junction curvature radius.

When the Rayleigh value is low the pseudo conduction mode dominates the heat transfer throughout the entire space, but as the Rayleigh number increases, the flow becomes increasingly apparent in the form of close intense counter rotating cells; the convective flow develops and takes over with a significant intensity in the solar chimney.

Furthermore the influence of the junction’s curvature geometry on the natural convection was also examined, it was found that the solar chimney with the maximum curvature radius Rc=0.54 is the optimum geometry in our case that could achieve the highest efficiency under the maximum vertical velocity. We concluded that the performance of a solar chimney is strongly correlated to the radius variation and the kinetic energy depends on the gap diameter of the junction.

Finally, the results from the collector’s height investigation revealed that a higher the collector goes the smoother and faster can the airflow develops within the whole space of the solar chimney. This research also helped us to determine the best location for the turbines to achieve the maximum efficiency.

In order to maximize the efficiency of the solar chimney and cut costs, we may enhance this study in the future by doing in-depth research on the effects of the chimney’s height and size and determining the impact of airflow velocity from the inlets.

References

[1] https://www.irena.org/Energy-Transition/Technology/Wind-energy 11/12/2022

[2]https://www.cleanenergywire.org/news/design-germanys-wind-power-distance-rules-undecided-vexation-over-policy-grows 11/12/2022

[3] Field, C. B., Campbell, J. E., & Lobell, D. B. (2008). Biomass energy: the scale of the potential resource. Trends in ecology & evolution, 23(2), 65-72.

[4] Hall, D. O. (1991). Biomass energy. Energy policy, 19(8), 711-737.

[5] https://education.nationalgeographic.org/resource/biomass-energy 11/12/2022
[6] https://www.researchgate.net/figure/Hydroelectric-Dam-Diagram_fig3_358572364 12/12/2022
[7] https://www.energy.gov/eere/fuelcells/fuel-cells 12/12/2022

[8] Vita-Finzi, C. (2008). The sun: A user's manual. Springer Science & Business Media.

[9]https://www.smart-energy.com/industry-sectors/business/edf-renewables-acquires-100-stake-in-us-based-entersolar/ 12/12/2022

[10] Abbas, R., Montes, M. J., Rovira, A., & Martínez-Val, J. M. (2016). Parabolic trough collector or linear Fresnel collector? A comparison of optical features including thermal quality based on commercial solutions. Solar energy, 124, 198-215.

[11] Al-Kayiem, H. H., & Aja, O. C. (2016). Historic and recent progress in solar chimney power plant enhancing technologies. Renewable and Sustainable Energy Reviews, 58, 1269-1292

[12] Vijayan, P. K., Nayak, A. K., & Kumar, N. (2019). Single-Phase, Two-Phase and Supercritical Natural Circulation Systems. Woodhead Publishing.

[13] Zhou, X., Wang, F., & Ochieng, R. M. (2010). A review of solar chimney power technology. Renewable and Sustainable Energy Reviews, 14(8), 2315-2338.

[14]http://www.actinnovation.com/innovation-environnement/energie-technologie-tour-solaire-800-metres-2716.html 16/12/2022

[15] Bello, R. S., Ezebuilo, C. N., Eke, K. A., & Adegbulugbe, T. A. (2015). Performance characteristics of modelled tri-wing solar chimney and adaptation to wood drying. Solar Radiation Applications, 53-71.

[16]https://www.boydcorp.com/resources/resource-center/blog/buoyancy-drives-natural-convection.html 17/12/2022

[17]https://www.researchgate.net/figure/Schematic-Diagram-of-Solar-Chimney_fig11_260479826 21/12/2022

[18] https://www.researchgate.net/figure/Schematic-of-roof-solar-chimney_fig21_289694544 25/12/2022

[19] Charitar, D. (2015). Numerical study of the thermal performance of solar chimneys for ventilation in buildings (Master's thesis, University of Cape Town).

[20] http://www.diva-portal.org/smash/get/diva2:971809/FULLTEXT01.pdf 26/12/2022

[21] Shi, L., **Zhang**, **G**., **Yang**, **W**., **Huang**, **D**., **Cheng**, **X**., **& Setunge**, **S**. (2018). Determining the influencing factors on the performance of solar chimney in buildings. Renewable and Sustainable Energy Reviews, 88, 223-238.

[22] Zhang, H., **Tao**, **Y**., **& Shi**, **L**. (2021). Solar chimney applications in buildings. Encyclopedia, 1(2), 409-422.

[23] Al-Kayiem, H. H., & Heng, Y. M. (2015). Experimental investigation of rooftop solar chimney for natural ventilation. Journal of Engineering and Applied Sciences, 10, 10249.

[24] Papageorgiou, C. (2010). Floating solar chimney technology. Solar energy, 187-222.

[25] https://ijtre.com/wp-content/uploads/2021/09/2020070520.pdf 26/12/2022

[26] Mohamad, H., Medhat, E., Mohamed, R., & Muthu, M. (2021). Use of Solar Chimney in Renewable Energy Applications–A Review. Renewable Energy Research and Applications, 2(1), 117-128.

[27] Adenigba, Oluwaseun. Performance evaluation of a solar chimney power plant using computational fluid dynamics. (2019), DOI: 10.13140/RG.2.2.13630.13126

[28]https://www.ecosources.org/50-prototype-de-tour-solaire-cheminee-implantee-a-manzanares-en-1982 26/12/2022

[29] Hakim, M. S. (2017). Recherche d'une configuration optimale d'une centrale solaire à cheminée (Doctoral dissertation, UNIVERSITE ABOU-BEKR BELKAID-TLEMCEN).

[30] http://www.reuk.co.uk/wordpress/solar/200mw-solar-tower/ 26/12/2022

[31]https://www.scmp.com/news/china/article/1487659/solar-chimneys-may-help-solve-chinas-energy-woes 27/12/2022

[32]عمرون آمنة_ بن داود دنيا. (2020). (محاكاة عددية لتأثير الشكل الهندسي للمدخنة الشمسية على تدفق الهواء عبر عنفة تحويل الطاقة). شهادة ماستر أكاديمي, جامعة محمد بوضياف المسيلة-المسيلة.

[33] BOUALLEG SALIM, **M**. (2012). Analyse des performances énergétiques des centrales cheminées solaires par utilisation de différents modèles mathématiques (Doctoral dissertation, Ecole Nationale Polytechnique).

[34] Kasaeian, A., Ghalamchi, M., & Ghalamchi, M. (2014). Simulation and optimization of geometric parameters of a solar chimney in Tehran. Energy conversion and management, 83, 28-34.

[35] Chergui, T., Larbi, S., & Bouhdjar, A. (2010). Thermo-hydrodynamic aspect analysis of flows in solar chimney power plants—A case study. Renewable and Sustainable Energy Reviews, 14(5), 1410-1418.

[36] Toghraie D, Karami A, Afrand M, Karimipour A, Effects of geometric parameters on the performance of solar chimney power plants, Energy (2018), doi: 10.1016/ j.energy.2018.08.086.

[37] AKCHICHE, Z. (2011). Etude de comportement d'une cheminée Solaire en vue de l'isolation thermique (Doctoral dissertation).

[38] Al-Taie, A. K., & Mutib, A. H. (2015). THE EFFECT OF ENTRANCE REGION GEOMETRY ON SOLAR CHIMNEY POWER PLANT PERFORMANCE. Muthanna Journal of Engineering and Technology (MJET), 3(2).

[39] Abdelsalam, **E**., **Kafiah**, **F**., **Almomani**, **F**., **Tawalbeh**, **M**., **Kiswani**, **S**., **Khasawneh**, **A & Alkasrawi**, M. (2021). An innovative design of a solar double-chimney power plant for electricity generation. Energies, 14(19), 6235.

[40] Rashid, **F**. **L**., & **Alnomani**, **S**. **N**. (2016). Effect of Spiral Rib on Solar Chimney Collector Performance. Al-Qadisiyah Journal For Engineering Sciences, 9(3), 349-359.

[41] Al-Taaie, **A**. **K**., **Mohammad**, **W**. **S**., **& Jubear**, **A**. **J**. (2016). Numerical simulation of the collector angle effect on the performance of the solar chimney power plant. Al-Khwarizmi Engineering Journal, 12(2), 79-89.

[42] Gahgah, **M**. (2008). Influence des régimes d'écoulement sur les performances énergétiques des cheminées solaires (Doctoral dissertation, Alger, Ecole Nationale Polytechnique).

[43] Comsol Multiphysics quick start and quick reference book version 3.5a © copyright 1998–2008

Abstract

The presented work concern a bi-dimensional numerical computation of a laminar airflow generated by natural convection within the solar chimney. The mathematical model was described by continuity, momentum and energy equations in the cylindrical coordinates system using Boussinesq's approximation. The simulation was performed with Comsol Multiphysics software. Results showed that the solar chimney's performance is strongly correlated to Rayleigh number and to the chimney geometrical proprieties as the junction curvature radius and the collector height.

Keywords: Natural convection, solar chimney, Boussinesq's approximation, numerical simulation.

ملخص

يتعلق العمل المقدم بحساب رقمي ثنائي الأبعاد لتدفق الهواء الصفيحي الناتج عن الحمل الحراري الطبيعي داخل المدخنة الشمسية. تم وصف النموذج الرياضي من خلال معادلات الاستمرارية والزخم والطاقة في نظام الإحداثيات الأسطوانية باستخدام تقريب بوسينسك. تم إجراء المحاكاة باستخدام برنامج Comsol Multiphysics وأظهرت النتائج أن أداء المدخنة الشمسية يرتبط ارتباطًا وثيقًا برقم رايلي والخصائص الهندسية للمدخنة مثل نصف قطر إنحناء الوصلة وارتفاع المجمع.

الكلمات المفتاحية: الحمل الحراري الطبيعي، المدخنة الشمسية، تقريب بوسينيسك، المحاكاة العددية.

Résumé

Le travail présenté concerne un calcul numérique bidimensionnel d'un écoulement laminaire généré par convection naturelle au sein de la cheminée solaire. Le modèle mathématique a été décrit par les équations de continuité, de quantité de mouvement et d'énergie dans le système de coordonnées cylindriques en utilisant l'approximation de Boussinesq. La simulation a été réalisée avec le logiciel Comsol Multiphysics. Les résultats ont montré que la performance de la cheminée solaire est fortement corrélée au nombre de Rayleigh et aux propriétés géométriques de la cheminée comme le rayon de courbure de la jonction et la hauteur du collecteur.

Mots clés : Convection naturelle, cheminée solaire, approximation de Boussinesq, simulation numérique.